# Testing the Limits of the BOPHY Platform: α, β, and Meso-derivatives.

A THESIS SUBMITTED TO THE FACULTY OF THE UNIVERSITY OF MINNESOTA BY

Alexander James King

IN PARTIAL FULFILLMENT OF THE REQUIREMENTS FOR THE DEGREE OF MASTER OF SCIENCE

Advised by Dr. Paul Kiprof

May 2019

**Acknowledgements**

I would like to thank Dr. Kiprof and Dr. Nemykin for giving me the opportunity to work in their labs for my undergraduate and graduate career. Without their guidance and support I don't think I would have found my love for chemistry. I would also like to thank Dr. Yuriy Zatsikha for being patient and working alongside me to teach me spectroscopic and synthetic techniques.

## Abstract

Due to the highly fluorescent nature of BOPHY it was hypothesized that this molecule would be good at light harvesting and electron transfer. The first organometallic BOPHY was synthesized and characterized using UV-Vis spectroscopy, voltammetry, and spectroelectrochemistry. These results were correlated with density functional theory (DFT) and time-dependent DFT (TD-DFT) computational methods. It was discovered that there is long range communication between the iron centers over 17 angstroms. Our second study investigated the stability of the BOPHY molecule when subjected to various functional groups. Using UV-Vis spectroscopy, NMR, HRMS and computational data, we have been able to conclude that the cyanation of BOPHY leads to a product that readily decomposes.

## Table of Contents

## List of Tables

## List of Figures:

**Figure from Chapter 1:**



**Figures from Chapter 2:**



**Figures from Appendix A:**



**Figures from Chapter 3:**

**Figures from Appendix B:**

# List of Compounds

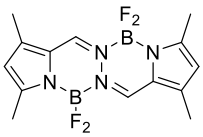

**(1)**

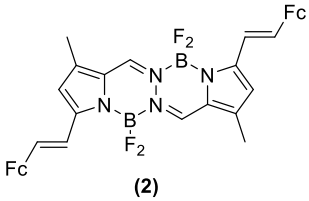

**(2)**

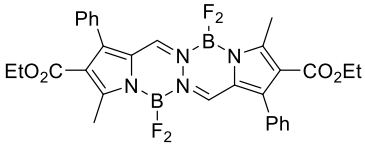

**(3)**

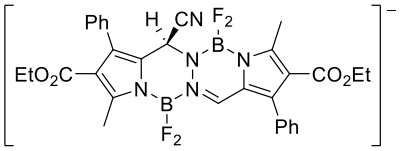

$K^+$18CR6

**(4)**

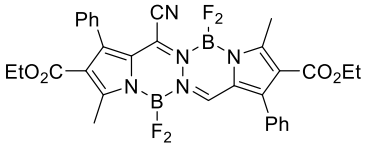

**(5)**

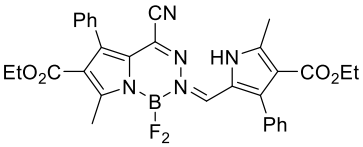

**(6)**

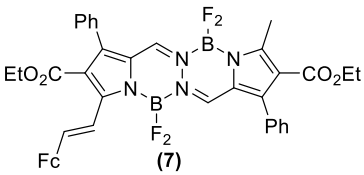

**(7)**

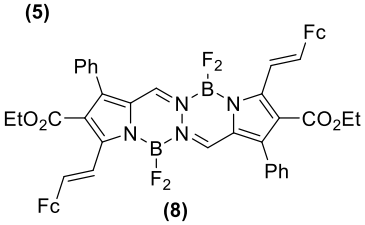

**(8)**

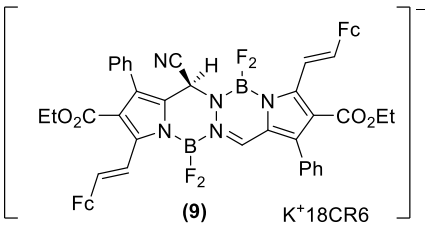

$K^+$18CR6

**(9)**

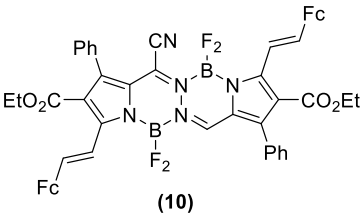

**(10)**

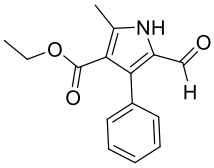

**(a)**

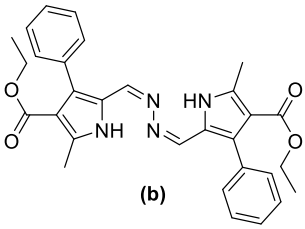

**(b)**

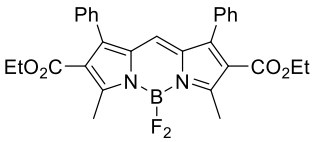

**(11)**

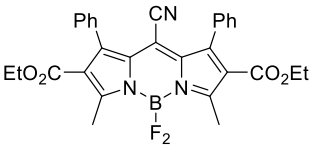

**(12)**

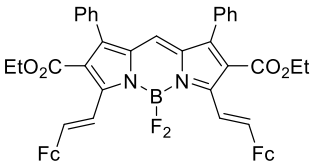

**(14)**

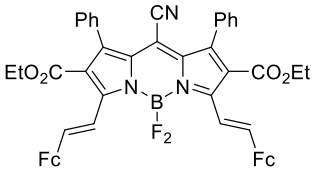

**(13)**

# Chapter 1

## Introduction:

A brief review of the history of BOPHY:

In 2014, the BOPHY platform was first published by Ziegler's group from the University of Akron.[1] This molecule is analogous to the world famous BODIPY (**bo**ron **dipy**rrolemethene). BODIPY is two pyrrole groups linked together with a methene and difluoroboron bridge, while BOPHY has two pyrrole groups linked together with a methene/hydrazine and difluoroboron bridge.[2–7] Due to these bridges the structure is a rigid, symmetric, quaternary ring based molecule. The IUPAC name for BOPHY is bis( difluoroboron) 1,2-bis((1H-pyrrol- 2yl) methylene) hydrazine. [1]

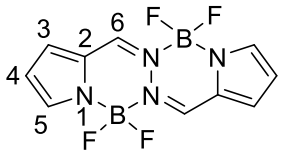


Figure 1.1: The conventional naming structure for BOPHY, where one side is label n, the opposite side is label n'.

When talking about substitutions on BOPHY, it's generally referred to by the position of substitution, (i.e. on 5, 5'). Another way to name BOPHY derivatives is by the naming system of porphyrins, BODIPY, and aza-BODIPY; the 5, 5' is referred to as the α-position, 3,3' the β-position, and 6,6' is the meso-position.

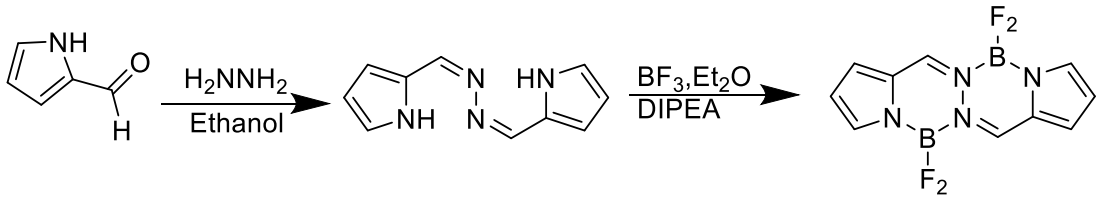


Figure l.2: Synthesis scheme for BOPHY

The BOPHY core can be made simply in a two-step process. First, a Schiff-base ligand is made by taking two equivalents of the pyrrole aldehyde with one equivalent of hydrazine hydrate in ethanol and stirring for two to three hours. This product precipitates out as a yellow solid that can be filtered off. The Schiff-base product is then reacted with two equivalence of $BF_3$•$Et_2O$ to form the final BOPHY product.

Fluorescent compounds and organic chromophores with intense board absorption bands in the near-infrared have always been attractive due to their application in light harvesting, bio-imaging, photodynamic therapy, and chemical sensors.[8–13] High stability, molecular extinction coefficients, and fluorescence quantum yields always been sought after when studying these types of chromophores and is why BODIPYs and aza-BODIPYs has found its success.[6,11]

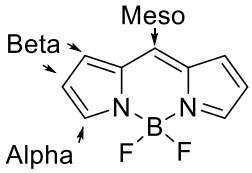


Figure 1.3: BODIPY naming system of alpha, beta, and meso positions.

The BODIPY's and aza-BODIPY's red-shifting, or reduction in the HOMO-LUMO gap, can be accomplished by the following: 1) introducing electron-donating groups at the α-pyrrolic positions,[18,21] 2) introduction of electron-withdrawing groups at the meso-

position,[21,22] 3) extension of the π-system in the chromophore's core.[23,24] Substitutions at the α-positions and extension of the π-system usually lead to a destabilization of the HOMO orbital (increases in energy). On the other hand, modification with electron withdrawing groups at the meso-positions usually leads a stabilization in the LUMO orbital (lowering the energy).[21,22] Synthetically, BODIPYs and aza-BODIPYs can be modified through coupling reactions, nucleophilic substitutions, or Knoevenagel condensations. BOPHY makes a good candidate for substitution to the BODIPY like structure and its strong physical properties. Ziegler's group reported BOPHY to have extinction coefficients for both unsubstituted and tetra-methyl substituted BOPHY to be over 37,000 $M^{-1}cm^{-1-}$ and have fluorescence quantum yields of 95 and 92% respectively.[1] Our work, as discussed in the following chapters, was centered around creating red-shifted BOPHYs with the following techniques: Knoevenagel condensation with the electron with donating group ferrocene, adding the cyano electron-withdrawing group at the meso position, and a combination of the two.

When it comes to multi-ferrocene substituted chromophores, our group has studied the redox properties of porphyrins, BODIPYs and aza-BOPHYs.[15,16, 18] More specifically a phenomenon known as intervalence charge transfer (IVCT). To summarize this briefly there according to Rob-Day, there are three classifications for intervalence charge transfer: Class i) redox sites are isolated and have their own oxidation/reduction. Class ii) redox sites have their own oxidation/reduction but readily interconvert. Class iii) redox sites become indistinguishable one another.[17] These classifications can be determined using the absorption spectra in an oxidized state and analyzing to determine if there is a

long board band formation in the low energy region. In addition to studying the BOPHY molecule's ability to have red-shifted absprptions, it was our goal to study to the metal to metal communication and investigate intervalence charge transfer on ferrocene substituted BOPHY molecules.

## Chapter 2:

## Unusually Strong Long-Distance Metal-Metal Coupling in Bis(ferrocene)-Containing BOPHY

### Introduction:

To understand the electronic properties of an organometallic BOPHY, the first of its kind was synthesized using a Knoevenagel condensation reaction with ferrocenecarboxaldehyde producing bis(ferrocene) BOPHY.[14] With our previous work done with bis(ferrocene) BODIPYs and aza-BODIPYs, showing electron coupling, our next goal with this new BOPHY was to study if there was electron coupling between the two ferrocene groups.[15,16]

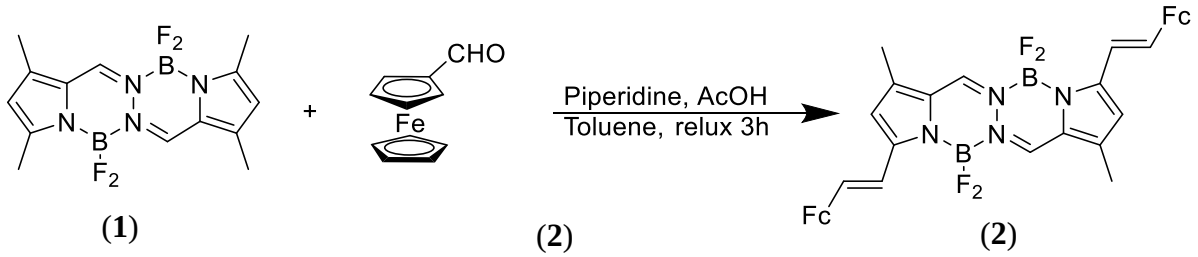


Figure 2.1: Synthesis scheme for bis(ferrocene) linked BOPHY at the 5,5' positions through vinyl bridges (**2**) from (**1**).

### Chemical Characterization:

The bis(ferrocene) BOPHY (**2**) was characterized using UV-Vis absorption spectroscopy and electrochemistry in dichloromethane solvent.

UV-Vis:

The parent tetra-methyl BOPHY had shown absorption peaks at 444 and 467 nm while extending the π-system on the new BOPHY with the conjugated ferrocene groups, results

in a bathochromic shift in to the near IR region. The maxima for the bis(ferrocene)BOPHY are found at 694, 564, and 343 nm. In typical ferrocene containing dyes, there tends to be a low intensity band in lower energy regions, which is indicative of metal-to-ligand charge transfer (MLCT). However, there is just a single band at 694 nm. To understand the electronic properties, DFT and TDDFT calculations were performed and will be discussed later.

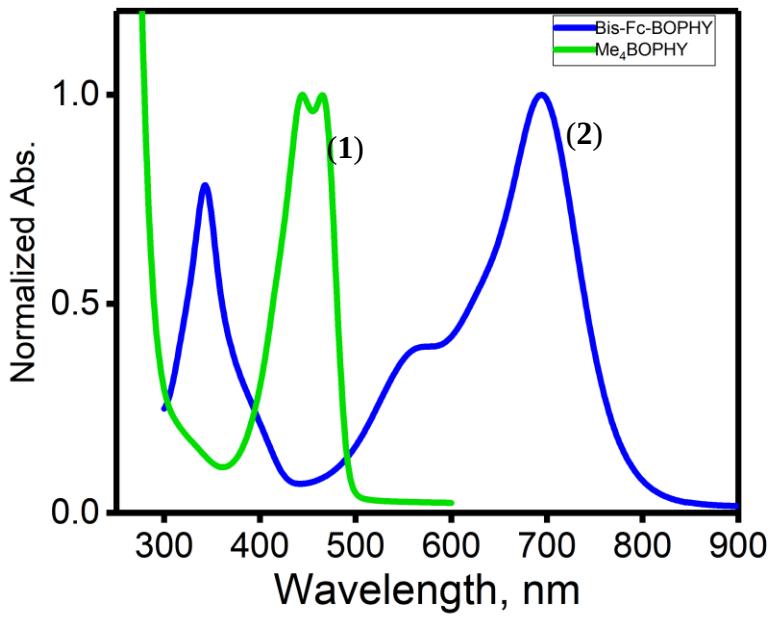


Figure 2.2: UV-Vis absorption spectra for the parent BOPHY (**1**) and bis(ferrocene)BOPHY (**2**).

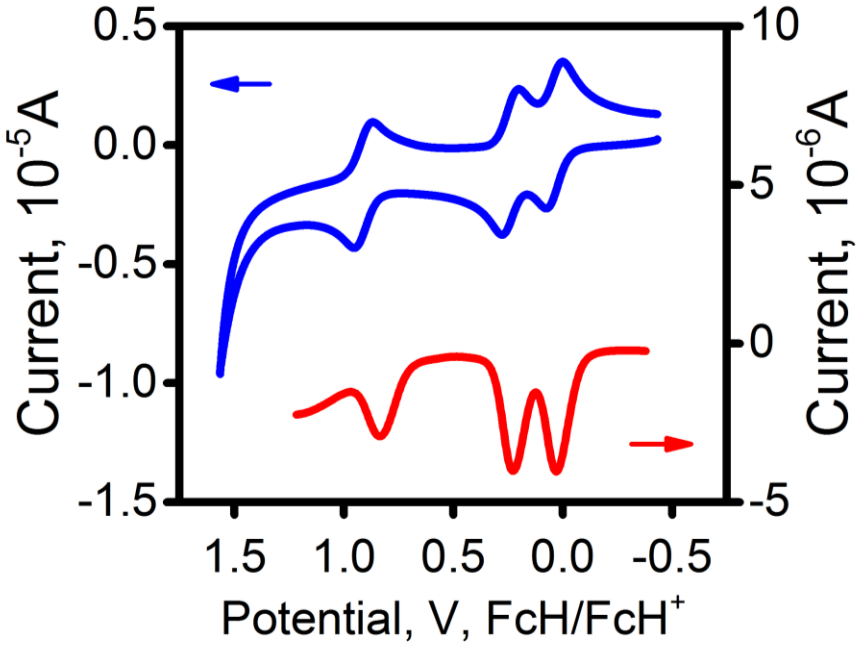


Figure 2.3: CV (top) and DPV (bottom) of bis(ferrocene)BOPHY (**2)** in DCM using TBAF as an electrolyte. Referenced to Fc/Fc$^+$.

Electrochemistry:

The oxidation processes for the BOPHY (**2**) were observed at 32, 236, and 906 mV (with respect to Fc/Fc$^+$) and no reduction processes were observed within the electrochemical window. Coupled with spectroelectrochemical experiments, the oxidations at 32 mV and 236 mV were assigned to the two ferrocenes and the oxidation at 906 mV to the BOPHY core. The 204 mV separation for ferrocene oxidation, is indicative that the two ferrocenes are communicating over a long distance. Based on the 17.2 Å distance of the two iron centers that is predicted through DFT calculations, the very large distance for communication is astounding and unexpected. However, it's not completely ruled out as an explication due to the rigidity and the π-system of BOPHY. To back up the claim that

there is communication between the two iron centers, spectroelectochemical and chemical oxidation experiments were performed.

Spectroelectrochemistry/chemical oxidation:

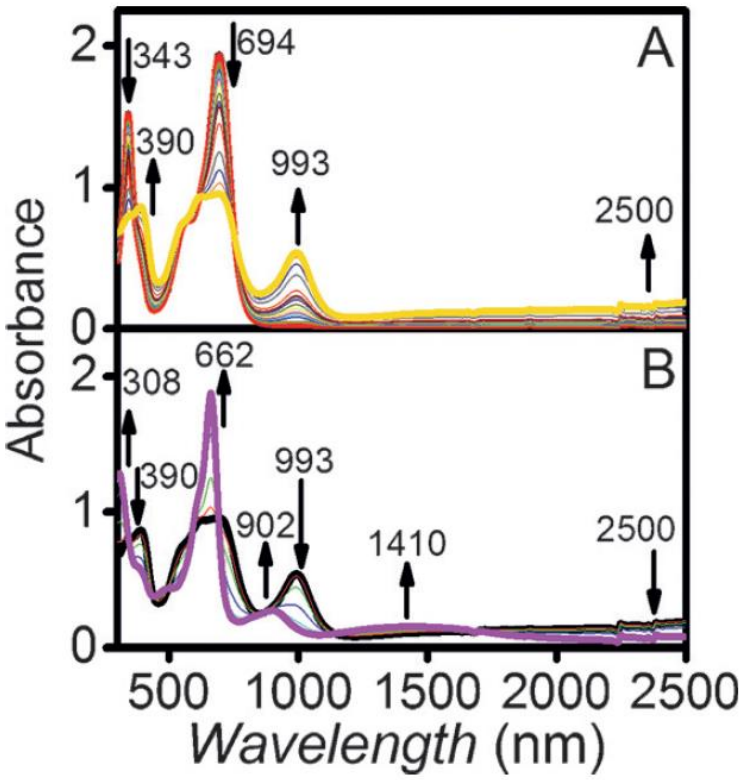


Figure 2.4: Spectroelectrochemical oxidations were (A) is the first oxidation and (B) is the second oxidation of (**2**).

The spectroelectrochemical and oxidation titration (appendix A) experiments were well in agreement with each other with similar band formation, band intensity loss, and band shifts. During the first oxidation, [BOPHY] → $[BOPHY]^+$, the bands at 2500 and 993 nm

begin to increase, the band at 694 nm begins to decrease, and the bands around 343 and 390 nm begin to decrease and increase, respectively.

The spectroscopic signature for communication of the two iron centers when one center undergoes oxidation is known as intervalence charge transfer (IVCT). It's common to see long/broad band formation in the NIR region. Although there are two band formations that occur under the first oxidation (993 and 2500 nm) and it appears that the band formation further in the NIR is indictive of IVCT, deconvolution analysis will help determine which band belongs to the IVCT process. Five peaks were found during the deconvolution analysis. Of the five bands that were found, the band at ~5000 $cm^{-1}$ was assigned as an IVCT band whereas the others are a mixture of LMCT and d-d transitions. Analysis of these band parameters were conducted using the band parameters using formulas (1) and (2):

$$H_{ab}=2.05\text{x}10^{-2}[(\upsilon_{max}\varepsilon_{max}\Delta\upsilon_{1/2})^{1/2}/r_{ab}] \quad (1)$$

$$\alpha^2=4.24\text{x}10^{-4}[(\varepsilon_{max}\Delta_{1/2})/(r_{ab}^2\upsilon_{max})] \quad (2)$$

From the analysis data, mixed-valence $[BOPHY]^+$ (**2**) was assigned to the Class II compound in Robin-Day classification. [17]

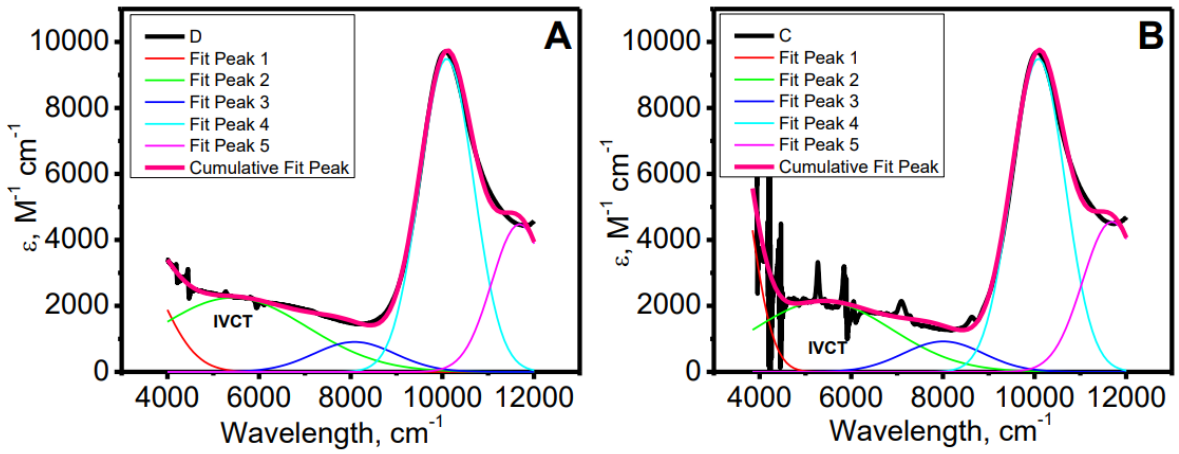


Figure 2.5: Deconvolution analysis of both the spectroelectrochemistry (**A**) and oxidative titrations (**B**). Labeling the IVCT band (green) at ~5000 $cm^{-1-}$.

**Computational Chemistry**

MO Analysis:

During the optimization process, the calculation yielded an energy difference of the $C_i$ and $C_2$ symmetries for the BOPHY (**2**) of 1.51 kcal/mol and would thus result in only minor differences in their electronic structures/vertical excitation energies. The HOMO to HOMO -10 molecular orbitals (MO) were calculated to be mostly on the ferrocene. Deeper into the molecular orbitals the HOMO -11 and HOMO -12 orbitals begin to be more BOPHY centered. If ferrocene is treated as Cp and $Fe^{2+}$ the HOMO, HOMO -4, and HOMO -7 molecular orbitals are between 33 to 44% contribution from just the iron alone. However, the HOMO -1 to HOMO -3 and HOMO -5/-6 are almost solely

ferrocene centered with predominate contribute from just the iron centers. Considering the LUMO orbitals, the LUMO and LUMO +1 orbitals are centered on the BOPHY core.

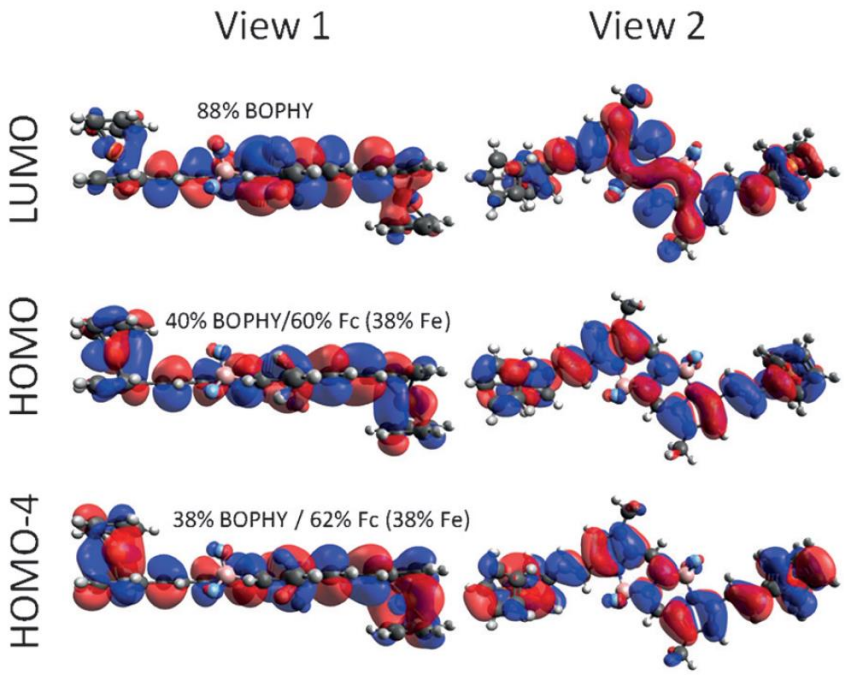


Figure 2.6: Molecule orbitals for $C_i$ symmetry for LUMO, HOMO, and HOMO -4 with a side (view 1) and top down (view 2) views of (**2**).

Table 2.1: MO composition analysis for $C_i$ symmetry of BOPHY (**2**).

| | | | % MO Composition | | | | |
|---|---|---|---|---|---|---|---|
| MO | Energy (eV) | Symmetry | N-N Bridge | BF2 | BOPHY | Fe | Cp |
| 183 | -5.341 | $a_g$ | 9.59 | 0.91 | 26.98 | 34.72 | 27.79 |
| 184 | -5.128 | $a_u$ | 0 | 0 | 0.43 | 67.59 | 31.98 |
| 185 | -5.128 | $a_g$ | 0 | 0 | 0.42 | 67.58 | 32 |
| 186 | -5.063 | $a_u$ | 0.79 | 0.17 | 8.26 | 58.19 | 32.59 |
| 187 | -4.846 | $\mathbf{a_g}$ | 9.78 | 0.73 | 30.42 | 37.42 | 21.66 |
| 188 | -2.997 | $\mathbf{a_u}$ | 6.94 | 1.41 | 79.53 | 5.6 | 6.52 |
| 189 | -2.066 | $a_g$ | 21.42 | 0.74 | 59.42 | 7.76 | 10.66 |
| 190 | -1.257 | $a_u$ | 1.27 | 0.24 | 56.03 | 19.17 | 23.29 |
| 191 | -1.066 | $a_g$ | 10.51 | 0.97 | 51.41 | 17 | 20.11 |
| 192 | -0.768 | $a_u$ | 0 | 0 | 0.99 | 41.06 | 57.95 |

| | | | | | | | |
|---|---|---|---|---|---|---|---|
| 193 | -0.768 | $a_g$ | 0.01 | 0 | 1.02 | 41.05 | 57.91 |

TDDFT Analysis:

Preforming TDDFT calculation on the bis(ferrocene) BOPHY, the resulting TDDFT-predicted UV-Vis spectra ($C_i$ and $C_2$ symmetries) are in agreement with the obtained experimental UV-Vis spectrum.

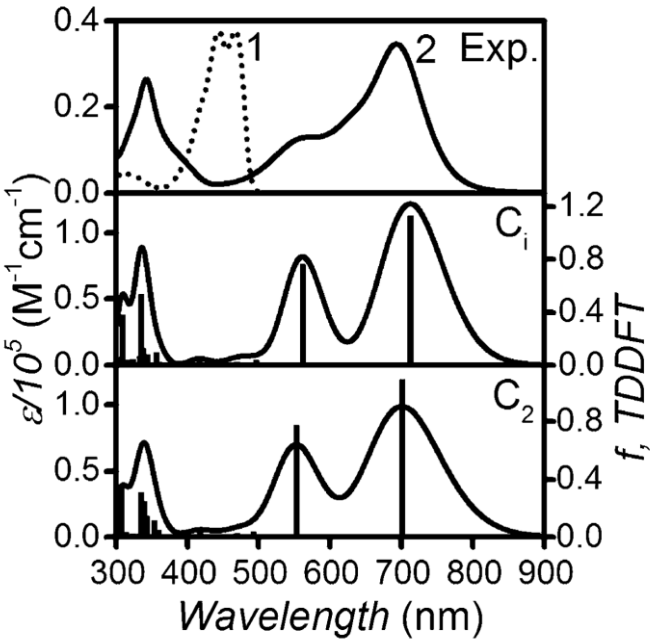


Figure 2.7: TDDFT-Predicted spectra of $C_i$ and $C_2$ symmetries (middle and bottom) and experimental spectra of $Me_4$BOPHY (**1**) and bis(ferrocene)BOPHY (**2**).

The TDDFT predicts the two bands in the low energy region (~550 and 700 nm) that are composed of excited states 1 and 5 for both symmetries. Where excited state 1 is primarily a HOMO → LUMO, single electron transition. The transition has a mixed $\pi$- $\pi^*$ and MLCT characters. Excited state 5 is primarily HOMO -4 → LUMO, single electron

transition, having the same character as the first excited state. The third band observed at ~330 nm is a predominantly π- $\pi^*$ transition from MOs HOMO -11/-12 → LUMO.

**Table 2.2:** TDDFT analysis summary table for $C_2$ and $C_i$ bis(Fc)BOPHY

| Excited State | Energy/nm($cm^{-1}$ ) | Symmetry | Oscillator Strength | Contributions |
|---|---|---|---|---|
| 1 | 700(14300) | $A_g$ | 1.1293 | Fe (37%), Cp(22%) --> BOPHY (80%) |
| 5 | 550(18200) | $A_u$ | 0.7599 | Fe (62%) --> BOPHY (80%) |

## Chapter 3

## Testing the Limits of the BOPHY Platform: Preparation, Characterization, and Theoretical Modeling of BOPHYs and Organometallic BOPHYs with Electron-Withdrawing Groups at β-Pyrrolic and Bridging Positions

Due to the attractive nature of BODIPY substitutions as discussed in the introduction, our next goal was to perform modifications on the BOPHY platform via cyanation at the meso-positions without affecting the stability of BOPHY.[20]

**Synthesis:**

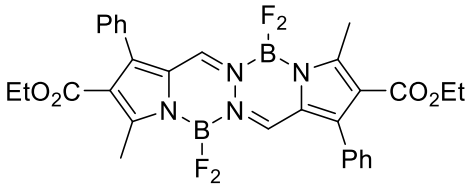


**(3)**

Figure 3-1: Structure of parent BOPHY (**3**).

Our first approach was to make a new BOPHY substituted at 4,4' with ester groups and 3,3' with phenyl groups (**3**). This was done by taking the already substituted 2-methyl-3-carbethhoxy-4-phenyl-pyrene and doing a formylation reaction to produce the pyrrole carboxaldehyde **a**. By adding hydrazine, the aldehyde underwent a condensation reaction to produce the Schiff base ligand **b**. The final step was to produce BOPHY (**3**) by adding $BF_3$•$Et_2O$.

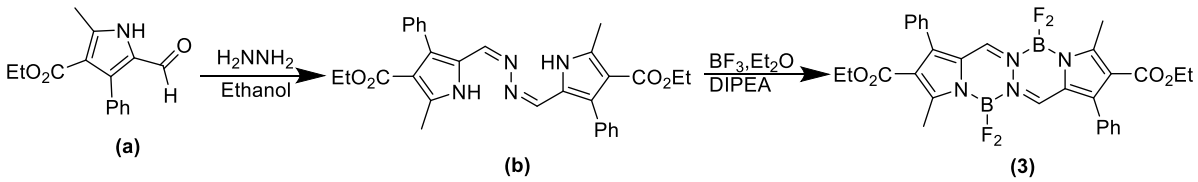


Figure 3-2: Scheme 3-1: Synthesis of **3**

Cyanation:

To cyanate the BOPHY platform, **b** was reacted with potassium cyanide in the presence of crown ether. Adduct **4** was successfully isolated and characterized, however, upon further oxidation to remove the proton at the meso-position, **5** decomposes back to **3** and to a new compound **(6)**. To try and produce the desired compound **(5)** the BOPHY salt was treated with various oxidants. The various oxidants used were (tris(4-bromophenyl) ammoniumyl hexachloroantimonate (magic blue), 2,3-dichloro-5,6-dicyanobenzoquinone (DDQ), N-bromosuccinimide (NBS), $Pb(OAc)_4$, and $Br_2$ in dichloromethane. All reactions produced an intense red colored solution that was stable enough to be characterized by UV-Vis spectroscopy. After about one hour the solution turns brown indicating decomposition of the compound. This process can be monitored qualitatively through TLC, the red spot (**5**) decomposes into 2 other spots: yellow (**3**) and brown (**6**)

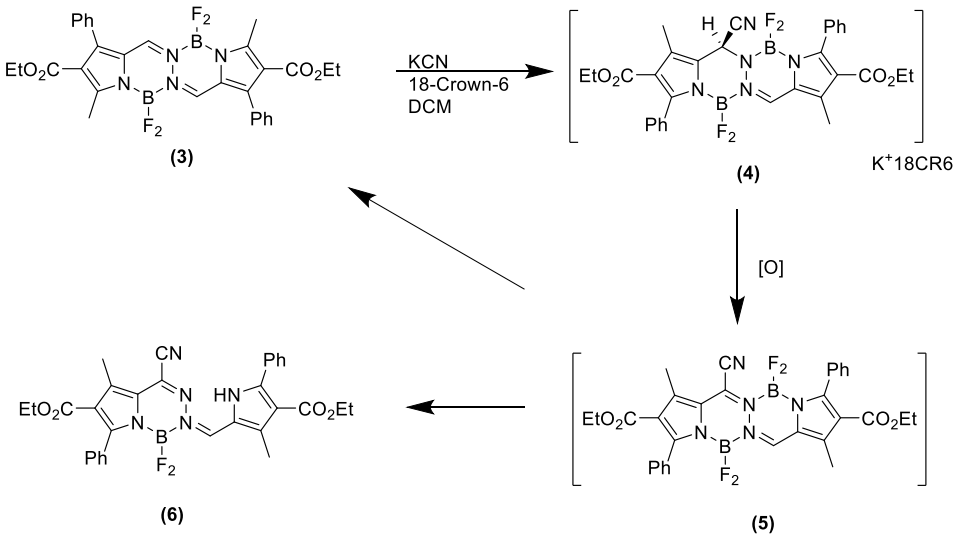


Scheme 3-2: Synthesis attempts to make a cyanated BOPHY **(5)**. Where [O] is an oxidant.

The decomposition of **5** is not completely unexpected due to the nature of the B-N bond. When adding an electron-withdrawing group at the meso-position the basicity of the adjacent nitrogen is decreased; that is, the ability for nitrogen to donate its electron pair is lowered. This would result in a weakened N-B bond, thus resulting in the formation of **6**.

One method we thought might work is introducing electron-donating ferrocene groups at the 5,5' positions, similar to what was discussed in chapter 2. The first step was to perform a test reaction on BODIPY; we took two approaches. With the starting BODIPY **(11)**, the chromophore was cyanated using the same reaction conditions for the cyanation of BOPHY (**3**). The resulting product was BODIPY **12** after oxidation. This product was then reacted with ferrocenecarboxaldehyde to produce the desired BODIPY **13**. The other method that was tested was to take BODIPY **11** and react it with ferrocenecarboxaldehyde to produce BODIPY **14**, this was then cyanated to give

BODIPY **13**. Both reactions worked, but with the latter method resulting in 80% yield overall compared to a 12% overall yield from the first method.

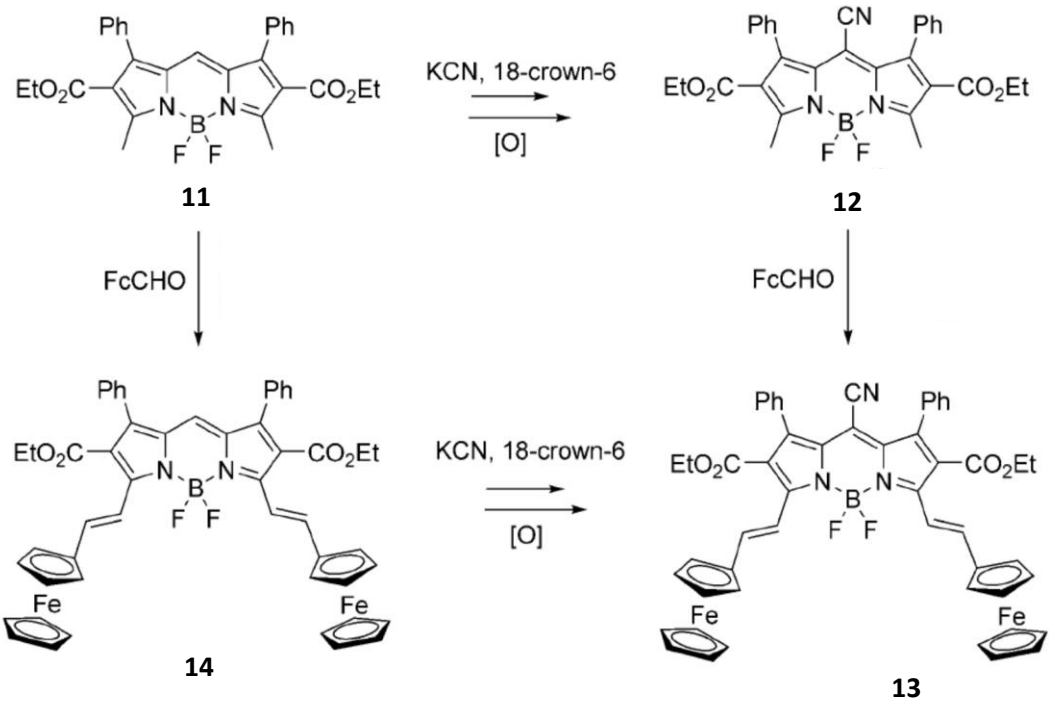


Scheme 3-3: Two synthetic routes to producing the desired cyanated compound.

With the successful isolation of cyanated BODIPY, our next goal was to isolate the cyanated BOPHY with ferrocene substitutions.

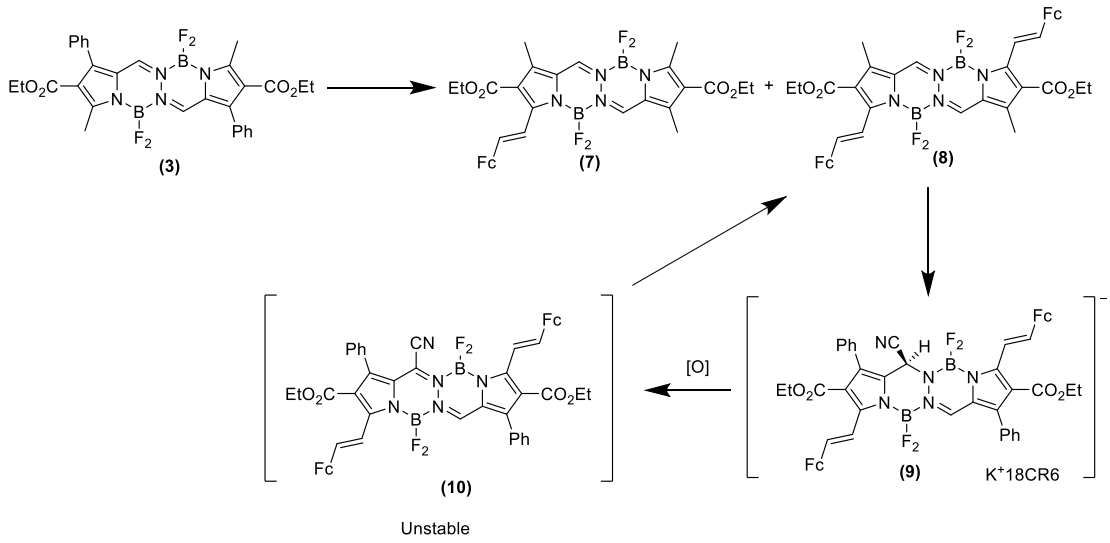


Scheme 3-4: Methodology for the synthesis of cyanated-ferrocene-BOPHY.

Similar to **(4)** we were able to isolate the BOPHY salt **9**, but upon oxidation, it decomposed back to **8**. As it appears, BOPHY has its limitations in that adding electron withdrawing groups at one of the meso-positions is an unfavorable transformation.

**Chemical Characterizations:**

All BOPHYs were characterized via $^{1}$HNMR, $^{13}$CNMR, UV-Vis spectroscopy and high-resolution mass spectrometry. Compound (**8**) characterized through X-ray crystallography (figure B.6.1 in appendix B)

Spectroscopy:

UV-Vis

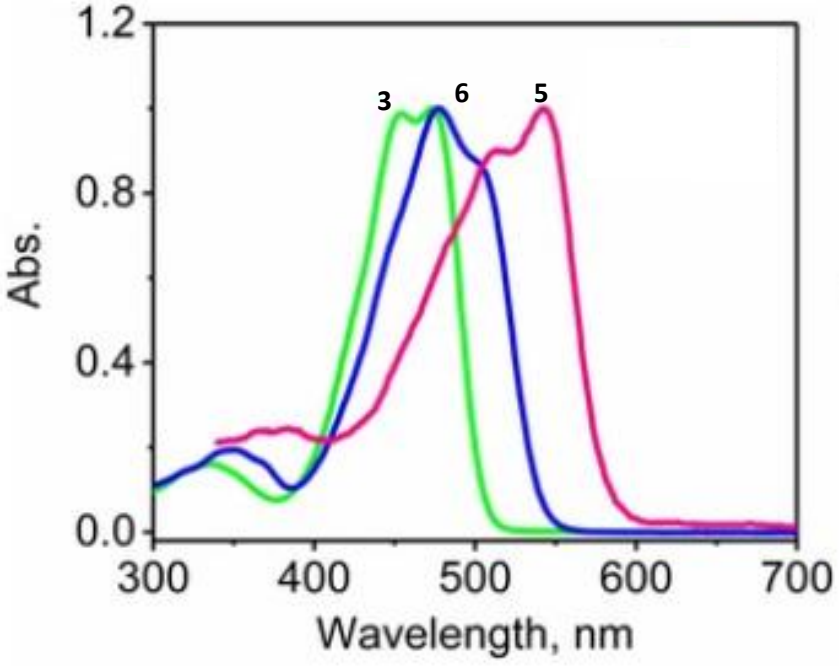


Figure 3-3: UV-Vis spectra for **3**, **5**, and **6** in DCM.

The UV-Vis spectra of **3**, **5**, and **6,** resemble similar band shapes of the simple BOPHY, where **3** being close to the simple BOPHY (**1)** (bands at 467 and 444 nm), there are bands at 473 and 454 nm for the new BOPHY. When the cyano group is attached at the meso-position (**5**) there is a significant shift of the bands to 542 and 510 nm which results in an average of 63 nm bathochromic shift from the original starting BOPHY. The "half-BOPHY" (**6**) we only see a slight shift with the bands residing at 505 and 478 nm.

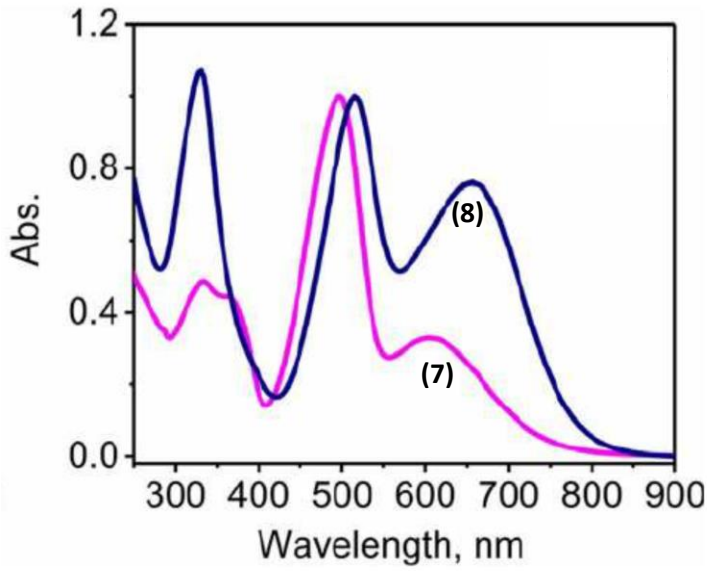


Figure 3-4: Experimental UV-Vis and TDDFT-predicted spectra for **7,** and **8** in DCM.

The UV-Vis spectra for **7** and **8** are similar in shape. The mono ferrocene substituted BOPHY (**7**) is blue-shifted and has a smaller band in the high energy region when the spectra are normalized. The two compounds have a narrow peak at 497 and 514 nm for **(7)** and **(8)**, respectively; additionally, both compounds also have broad peaks at 606 and 656 nm, respectively. As the π-system is extended through the vinyl bridges at the 5 and 5', there is a clear red shift of the π- π* transition. This transition of **3** at 474 nm shifts to 497 (**7**) with one extension and further shifts to 514 nm (**8**) with a second extension of the π-system.

Fluorescence:

The (**3)** and **(6)** compounds do not have mirrored excitation and emission spectra. The parent compound **(3)** has a prominent peak at 506 nm with a smaller shoulder at 538 nm; while the spectrum of **6** has a peak at 548 nm and a shoulder at 580 nm. The Stokes shifts for **3** and **6** were found to be large with values of 1650 and 1555 $cm^{-1}$, respectively. Just

like the original unsubstituted and tetramethyl substituted BOPHYs, **3** was found to have a very high fluorescence quantum yield (98%). When comparing **3** to **6**, the quantum yield for **6** is  approximately100 times lower (1.1%) The ferrocene substituted compounds had a fluorescence quenching effect due to the electron transfer properties of the ferrocene (see figurex.x in appendix B.

Redox properties:

Four of the compounds were studied with cyclic voltammetry (CV), differential pulse voltammetry (DPV), and spectroelectrochemistry: **3, 6, 7,** and **8.**

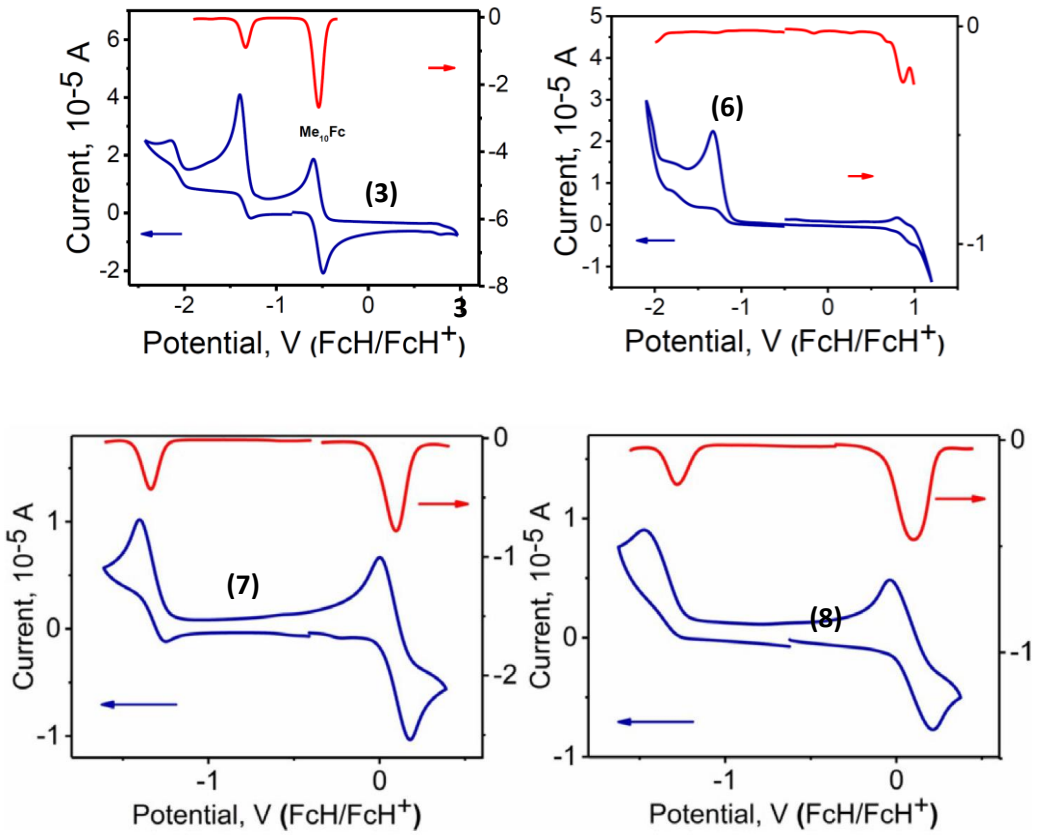


Figure 3-5: Redox data for **3, 6, 7,** and **8** in 0.1M TBAP/$CH_2Cl_2$ system. CV = blue, DPV = red.

In the parent molecule (**3**), there was no observed oxidation and one irreversible reduction at -1.34 V. The half-BOPHY (**6**), showed two irreversible oxidation and reduction processes. The ferrocene containing compounds (**7** and **8**) showed reversible oxidations +0.1 V relative to $Fc/Fc^+$. Both of mono and bis ferrocene compounds showed that the ferrocene groups oxidize at the potential, while the bis compound has a broader oxidation wave. Comparing to the compound in the previous chapter, where we observed a 200 mV separation of the ferrocene groups, the **8** compound has only a single oxidation wave, indicating a lack of electronic coupling.

Spectroelectrochemistry:

The first BOPHY that was studied was **7**; during the first oxidation the band at 600 nm disappears and the band at 491 nm undergoes a small hypsochromic shift to 485 nm. Additionally, during the first oxidation a band at 930 nm with low intensity begins to form, that has been observed for other vinylferrocene conjugated systems. This first oxidation is completely reversible, and the original spectral properties were restored with the reduction of the BOPHY from oxidized state.

The bis(ferrocene)BOPHY (**8**) had similar spectral changes as the mono ferrocene BOPHY. The MLCT band at 650 nm decreases, the major band at 523 nm shifts to 515 nm, and a band at 930 nm forms. Different from the original bis(ferrocene)BOPHY **(2)** (as discussed in chapter 2), there was a lack of observation of an IVCT band, indicating a lack of electronic communication between the iron centers. Currently, the main reason behind this lack of IVCT is not known, but it can be speculated that based on the ester/phenyl groups, there is additional conformational flexibility in the BOPHY system;

this could modify the electronic structure not allowing the electronic communication between two iron centers to take place.

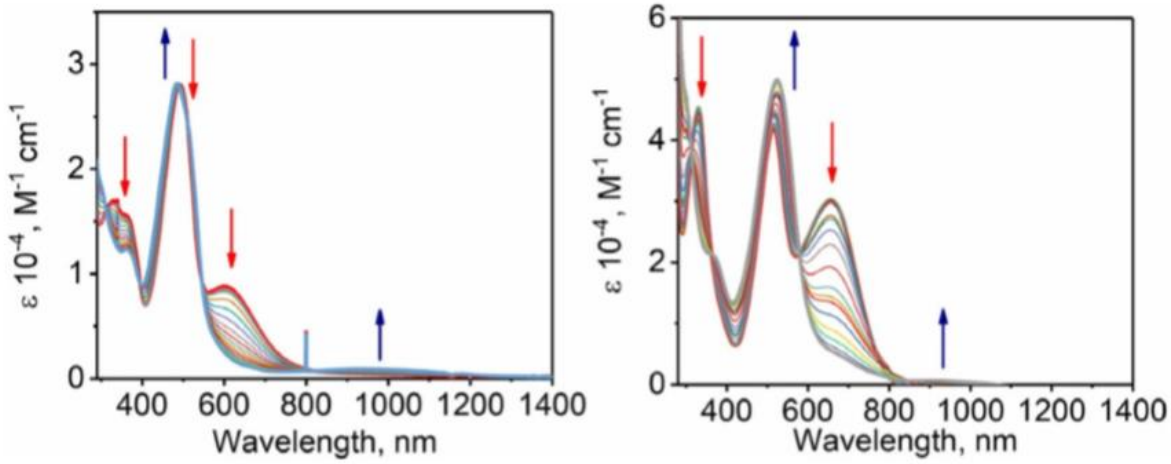


Figure 3-6: Spectroelectrochemcal oxidation of **7** (left) and **8** (right)

**Computational Studies:**

Computational modeling was used to understand the electronic structures and spectroscopic data as well as explain why the $BF_2$ group leaves during cyanation of **3**. DFT and TDDFT was used on all target compounds.

Looking deeper into the electronic structure of the BOPHY core, the bridging carbon next to the hydrazine bridge contributes to the LUMO orbital and not the HOMO (figure 3-7). Thus, adding in a cyano group here stabilizes the energy of the LUMO. The DFT calculations can predict the stepwise reduction of **3** → **5** → **6** which also explains the red shift that was observed in figure 3-3. Looking at the ferrocene BOPHYs, both the compounds have HOMO orbitals very close in energy (figure 3-8). These two

compounds also have a much lower HOMO-LUMO gap and would explain the low energy MLCT band observed in figure 3-4.

DFT calculations were also used to predict bond length changes upon cyantion of **3**, the B-N (pyrrole) bond length is not affected but the B-N(hydrazine) bond length experiences an extension of 0.03 Å. This extension leads to a weakened bond in the $BF_2$ fragment and would explain why the compound readily decomposes from **5** to **6**. Analyzing the Mulliken charges of the bridging carbon, in the case of the cyanated BOPHY, there is a large positive charge of 0.461; compared to the original BOPHY (**1**) (0.109). Looking at the B-N(hydrazine) bond, the charge on **5** is -0.349 and on **1** is -0.260. Thus, elimination of $BF_2$ which leads to compound **6**, the charge on the bridging carbon is reduced to +0.292 (from +0.461 on **5**). The lack of electron density explains the bond extension of B-N(hydrazine) and loss of $BF_2$.

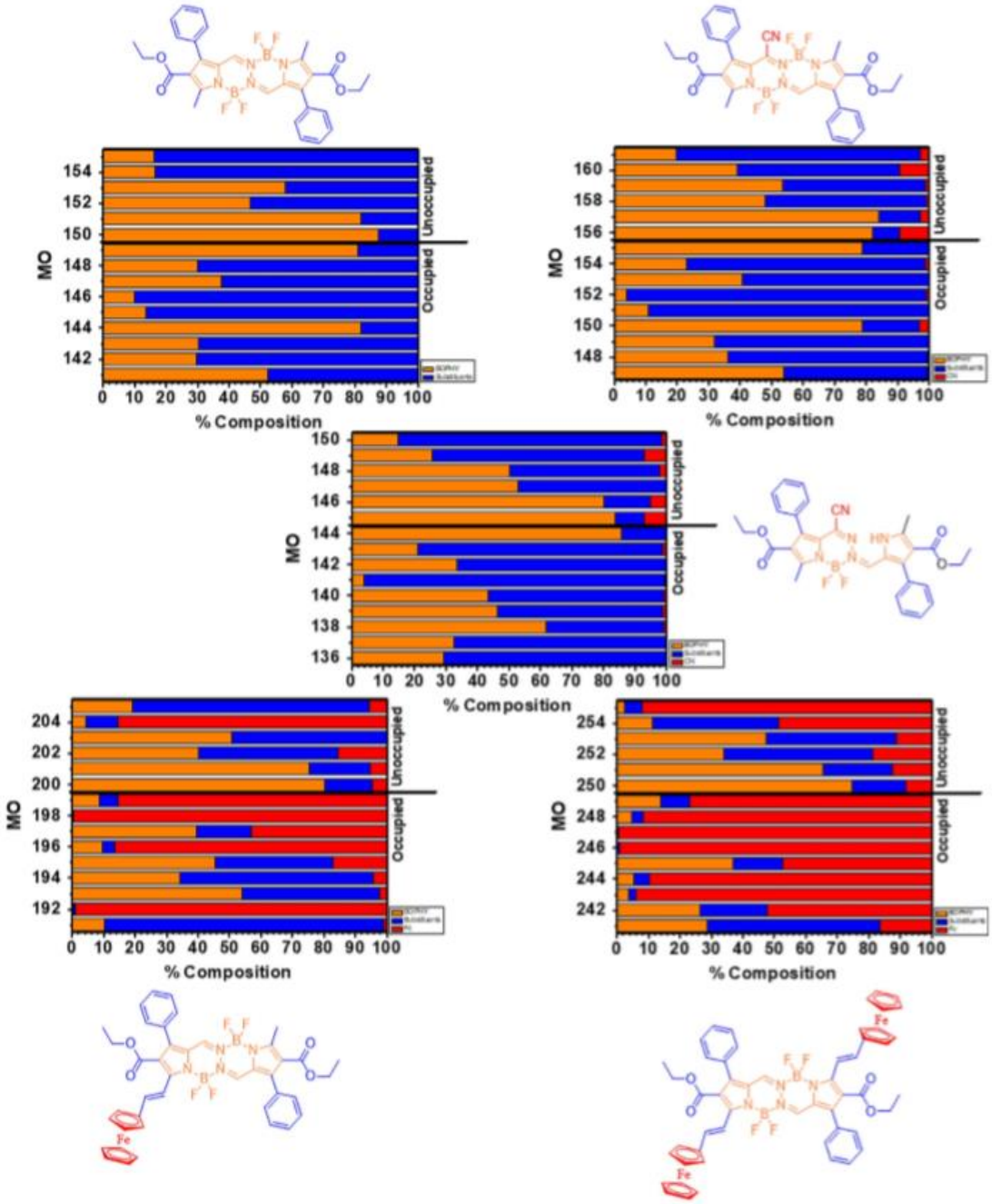


Figure 3-7: DFT molecular orbital composition (graphical)

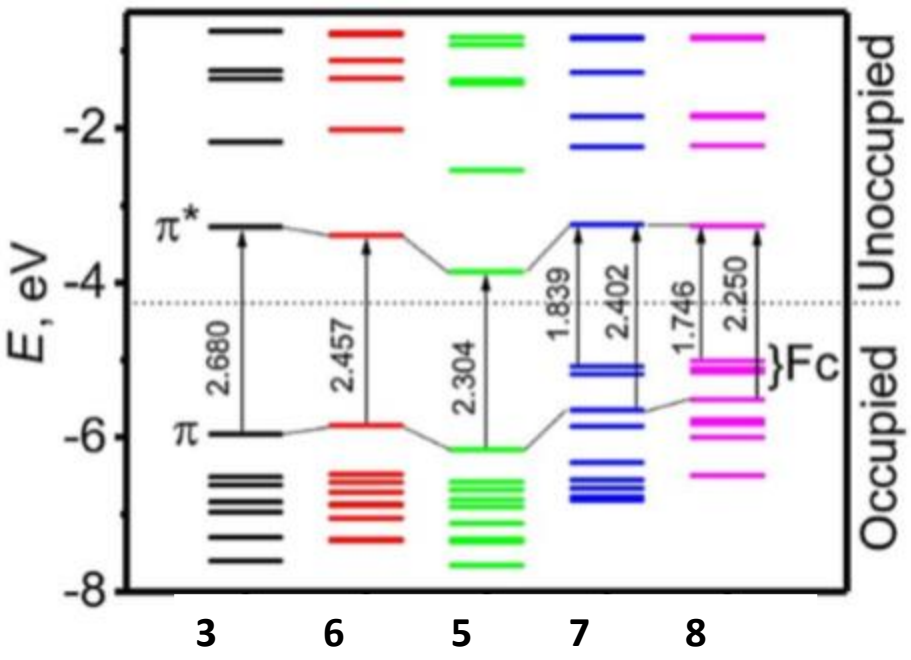


Figure 3-8: molecular orbital energies with HOMO-LUMO gap energies.

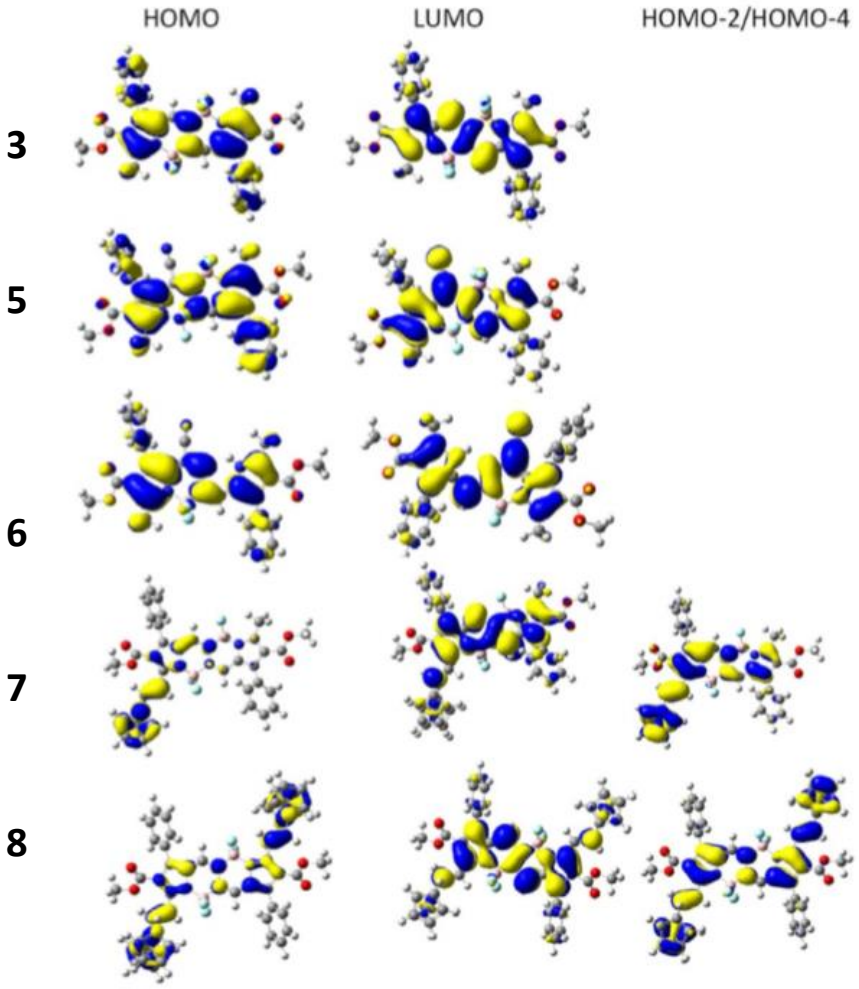


Figure 3-9: MO images of the BOPHY compounds

TDDFT:

All TDDFT calculations were conducted with the TPSSh hybrid exchange-correlation functional with the Wachters full-electron basis set for iron atoms and 6-311G(d) basis set for all other atoms. To model solvation effects, the PCM approach was used. The organic molecules had the first 30 excited states calculated, whereas the organometallic molecules had the first 50 excited states calculated.

TDDFT-predicted UV-Vis spectra of BOPHY compounds **(3, 6, 7,** and **8)** are compared to the experimental spectra in figure 3-10. The organic spectra BOPHYs (**3, 5,** and **6**) had spectra that had a single high intensity band what had π-π* character from the HOMO-LUMO transition. BOPHY molecules **5** and **6** had several low intensity bands at higher energy which had transitions from HOMO -1 → LUMO and HOMO -2 → LUMO. These transitions would explain why there is a broader band in the experimental spectra for these two compounds (figure 3-9).

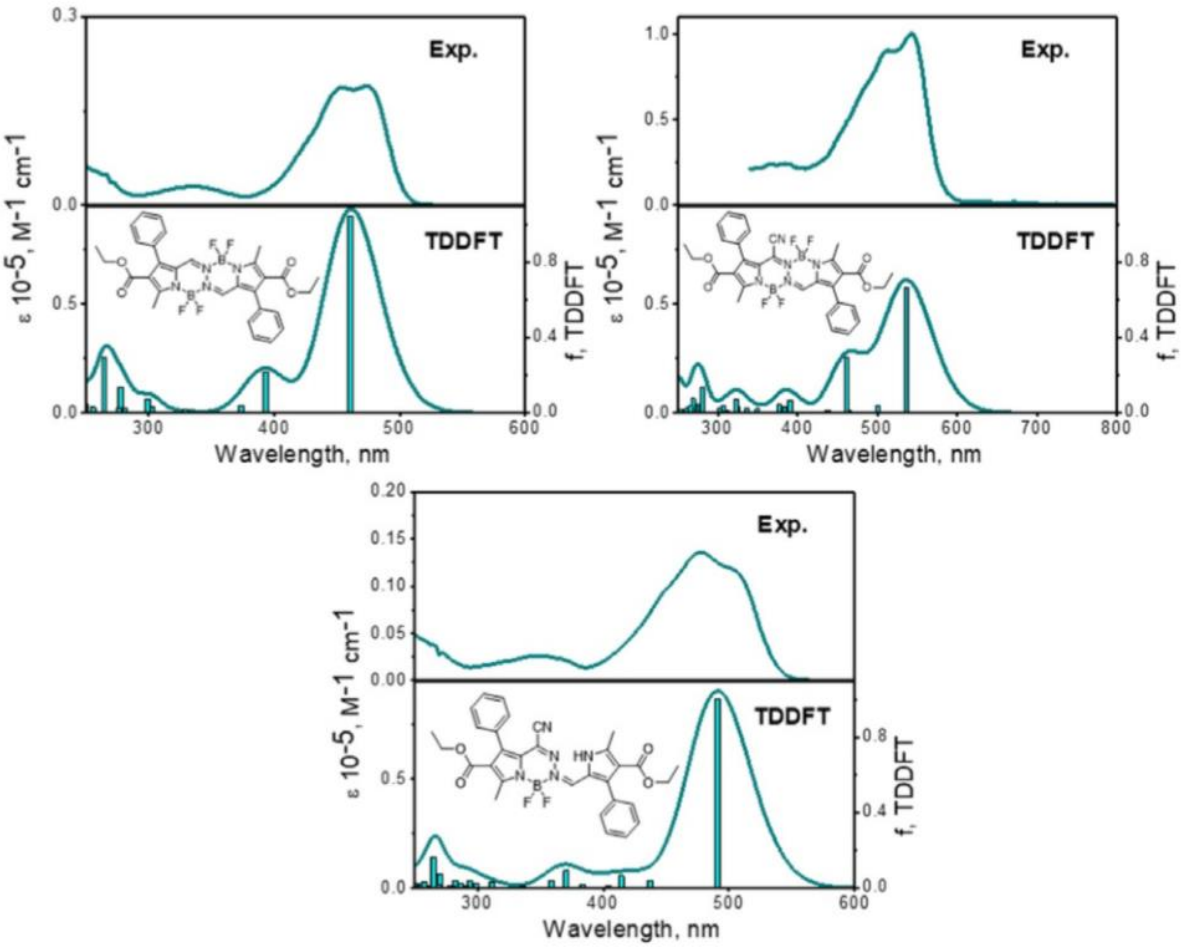


Figure 3-10: TDDFT with experimental spectra for the organic BOPHYs.

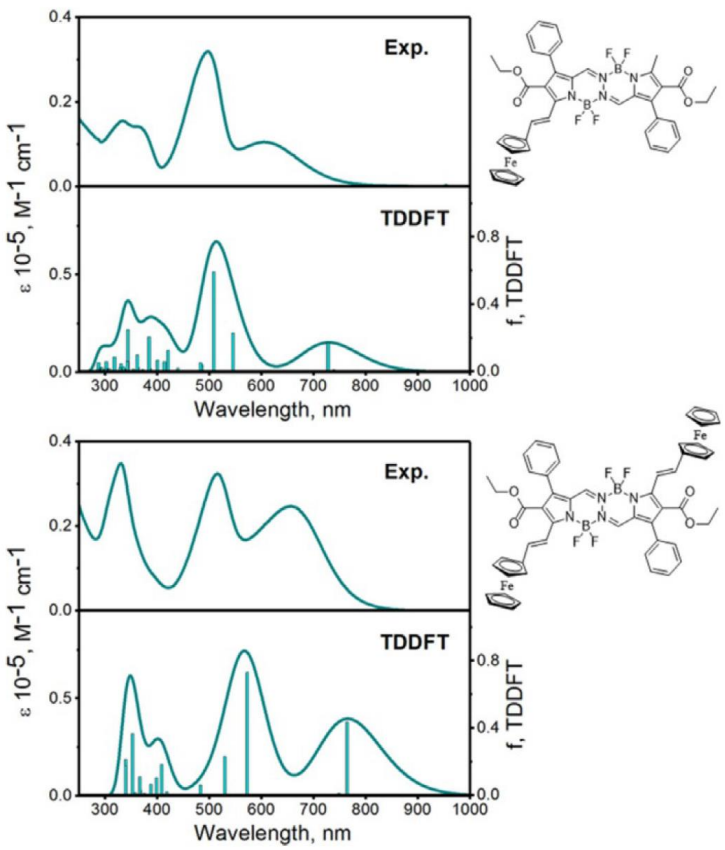


Figure 3-11: TDDFT with experimental spectra for the organometallic BOPHYs.

The organometallic BOPHYs **(7,8)** had a low-energy band that had mostly MLCT character from the HOMO-LUMO transition. The higher intensity band at slightly higher energy consisted of contributions from the HOMO -2 → LUMO and HOMO -4 → LUMO; these transitions were mostly π-π* in nature.

**Table 2.3:** TD-DFT analysis summary table for BOPHYs (3, 5, 6, 7, 8)

| | Excited State | Energy (nm) | Energy (cm-1) | Symmetry | Oscillator Strength | Transition Contributions |
|---|---|---|---|---|---|---|
| 3 | 1 | 461.30 | 21678 | $A_u$ | 1.0399 | HOMO (149) →LUMO (150) |
| | 3 | 393.96 | 25383 | $A_g$ | 0.2143 | HOMO -4 (145) → LUMO (150) |
| 5 | 1 | 537.59 | 18602 | A | 0.6605 | HOMO (155) →LUMO (156) |
| | 4 | 462.68 | 21613 | A | 0.2894 | HOMO-4 (150) → LUMO (156) |
| 6 | 1 | 491.19 | 20359 | A | 1.0021 | HOMO (144) → LUMO (145) |
| 7 | 2 | 728.97 | 13718 | A | 0.165 | HOMO (199) → LUMO (200) |

| | | | | | | |
|---|---|---|---|---|---|---|
| | 3 | 546.15 | 18310 | A | 0.223 | HOMO-2 (196) → LUMO (200), HOMO (199) → LUMO (200) |
| | 4 | 509.52 | 19626 | A | 0.5884 | HOMO-2 (196) → LUMO (200), HOMO -1 (197) → LUMO (200) |
| 8 | 1 | 765.87 | 13057 | $A_u$ | 0.4325 | HOMO (249) → LUMO (250) |
| | 5 | 573.54 | 17436 | $A_u$ | 0.7276 | HOMO-5 (243) → LUMO (250) |
| | 7 | 530.62 | 18846 | $A_u$ | 0.2248 | HOMO-5 (243) → LUMO (250) |

**Conclusion:**

New BOPHYs have been prepared with ester substitutions in the 4,4' positions and phenyl groups in the 3, 3' positions as a new BOPHY core. Ferrocene was attached at the 5,5' positions on the new BOPHY core, similar to our previous work. We have attempted to attach a cyano group at the 6, 6' position with unsuccessful results due to the instability of the compound due to low charge density of the substituted carbon atom as verified through DFT calculations. A new "half-BOPHY" was created in the process which is the loss of the $BF_2$ group. In addition to synthesis, spectroscopy and redox properties were used to characterize these new BOPHYs. DFT and TDDFT calculations were used to correlate our experimental data and understand the electronic properties on the BOPHYs.

# Chapter 4: Conclusion

As outlined in chapter 2, the first organometallic BOPHY was synthesized and characterized. With the ferrocene substitutions, we have found that the original compound's fluorescence is quenched and exhibits similar behavior to BODIPYs[18], aza-BODIPYs[15], and phthalocyanines[19] with analogous substitutions. The absorption bands were characterized using TDDFT calculations and it was found to be a mixture of π- π and MLCT character for the broad, low energy bands; while the high energy band was found to be primarily π- π in nature. Long-ranged metal-metal coupling over 17 Å with a 200 mV separation was observed through electrochemistry. Using spectroelectro-chemistry and chemical oxidations data, the mixed-valence of **[2]**$^{+}$ was assigned as a Class II compound in Robin-Day classification.

As described in chapter 3, new BOPHY compounds have been prepared with ethyl ester substitutions in the 4,4' positions and phenyl groups in the 3, 3' positions as a new BOPHY core. Ferrocene was attached at the 5,5' positions on the new BOPHY core, similar to compound **2** in chapter 2. We have attempted to attach a cyano group at the 6 position with unsuccessful results due to the resulting instability of the compound. The low charge density of the substituted carbon atom and lack of N-B covalent character contributed to this instability of compound **6**, as verified through DFT calculations. A new "half-BOPHY" was created in the process which is the loss of a $BF_2$ group. In addition to synthesis, spectroscopy and redox properties were used to characterize these new BOPHYs. DFT and TDDFT calculations were used to correlate our experimental data and understand the electronic properties on the BOPHYs. Unlike like the Class ii

that was found for the bis(Fc)BOPHY (2), there was no intervalence charge transfer band found for the similar compound, compound 8.

## Chapter 5: Experimental Procedures

**Experimental details:**

NMR spectra were recorded on a Bruker Avance Instrument with a 300 MHz Frequency for Protons and 75 MHz frequency for carbons. Chemical shifts are reported in parts per million (ppm) and referenced to tetramethylsilane (Si[CH3]4) as an internal standard. High-resolution mass spectra of all compounds were recorded using a Bruker microTOF-QIII. UV-Vis data was collected on a Jasco-720 spectrophotometer.

Fluorescence spectra were recorded on a Cary Eclipse spectrometer.

**Synthesis of 1:**

The Bis(ferrocene) BOPHY (**2)** can be prepared by using tetramethyl BOPHY ($Me_4$BOPHY) as the BOPHY of choice. The $Me_4$BOPHY (**1)** (80 mg, 0.24 mmol) and ferrocene carboxaldehyde (102 mg, 0.48 mmol) were dissolved in 20 mL of toluene. Piperidine (1 mL) and a catalytic amount of *p*-toluenesulfonic acid were mixed and a small portion of toluene then added to the mixture. The solution was then refluxed for 48 h while being monitored by TLC. After the disappearance of $Me_4$BOPHY the reaction was cooled to room temperature and the solvent was removed under vacuum. Using chromatography with silica gel and methylenechloride:hexane (50:50) the bis(ferroene)BOPHY was obtained at 4% yield (8 mg). The compound was characterized by $^{1}$H NMR, $^{13}$C NMR, $^{19}$F NMR:

$^{1}$H NMR (500 MHz, $CDCl_3$): δ (ppm) 2.30 (s, 6H, CH3-H), 4.20 (s, 10H, Cp-H), 4.44 (br s, 4H, β-Cp-H), 4.64 (br s, 4H, α-Cp-H), 6.63 (s, 2H, β-pyrr-H), 6.98 (s, 2H, meso-H), 7.12 (d, J = 16.0 Hz, vinyl-H), 7.25 (d, J = 16.0 Hz, vinyl-H)

$^{1}$H NMR (500 MHz, dmso-$d_6$, δ ppm): 7.57 (s, 2H, meso-H), 7.37 (d, 7.37 Hz, 2H, vinyl-H), 7.01 (d, 7.37 Hz, 2H, vinyl-H), 6.89 (s, 2H, β-pyrr-H), 4.62 (s, 4H, α-Cp-H), 4.53 (s, 4H, β-Cp-H), 4.21 (s, 10H, Cp-H), 2.30 (s, 6H, CH3-H).

$^{19}$F NMR (300 MHz, $CDCl_3$): δ (ppm) -139.77 (q, J B-F = 21.0 Hz)

$^{13}$C NMR (500MHz, $CDCl_3$): δ (ppm) 11.35, 68.11, 69.68, 70.45, 82.21, 115.14, 115.34, 117.21, 135.21, 136.44, 139.15, 153.45.

**Synthesis of (a)** 5-Formyl-2-methyl-4-phenyl-1H-pyrrole-3-carboxylic acid ethyl ester (2): The formylation of the pyrrole was carried out using a modification to a previously described procedure. $POCl_3$ (10.1 g, 65.8 mmol, 1.1 eq) was added dropwise into DMF (14 mL, 3 eq) solution in an ice bath, and stirred for 30 min at 0°C. Then, a solution of pyrrole 1 (13.7 g, 59.8 mmol, 1eq) in 45 mL of DMF was added, and the resulting mixture was left to stir for another 15 min. The resulting mixture was then heated in an oil bath at 85$^{o}$C for 1.5 h. The solution was then cooled down to room temperature, diluted with ice water (50 mL), and neutralized with $K_2CO_3$. The resulting precipitate was filtered off and dried. The crude product was recrystallized from acetonitrile, yielding 11.6 g (75%) of compound **a**. $^{1}$H NMR (300 MHz, [$D_6$] DMSO) d 12.54 (s, 1H), 9.13 (s, 1H), 7.38 (s, 5H), 4.04 (q, JH,H=7.1 Hz, 2H), 2.49 (s, 3H), 1.00 ppm (t, JH,H=7.1 Hz, 3H).

**Synthesis of b (**Schiff-base ligand): The mixture of pyrrole aldehyde **a** (900 mg, 3.5 mmol) in 20 mL of ethanol was heated at 60°C until the precipitate dissolved. Then hydrazine monohydrate (105 mg, 2.1 mmol) and a catalytic amount of glacial acetic acid were added to the reaction flask. The resulting mixture was stirred at room temperature for 2 h. The resulting yellow precipitate was filtered off, washed with a small amount of ethanol, and air-dried. The yield was 680 mg (75%). $^{1}$H NMR (300 MHz, $CDCl_3$): d 9.09 (s, 2H), 8.11( s, 2H), 7.37–7.30 (m, 10H), 4.11(q, $J_{HH}$=7.1 Hz, 4H), 2.58 (s, 6H), 2.33 (s, 6H), 1.07 ppm (t, $J_{HH}$=7.1 Hz, 6H); $^{13}$C NMR (75 MHz, $CDCl_3$): d 150.08, 139.63, 133.75, 133.13, 130.67, 127.61, 127.32, 124.12, 59.63, 14.24, 14.10 ppm; HRMS (APCI positive) calcd for $[M+H]^+$:511.2340, found 511.2443

**Synthesis of 3**: Schiff base **b** (3.5 g, 6.86 mmol) was dissolved in $BF_3{\cdot}Et_2O$(25 mL). Diisopropylethylamine (DIPEA) (14.4 mmol, 1.85 g, 2.51 mL) was then added dropwise into the solution. The resulting mixture was stirred for 1h at 80°C in an oil bath. After cooling to room temperature, the solution was slowly added into cold methanol (30 mL) and stirred for another 30 min. The resulting precipitate was filtered as a fluorescent orange powder to give 3.30g (yield 80%) of pure product (**3)**. $^{1}$H NMR (300 MHz, $CDCl_3$): d 7.85 (s, 2H), 7.48–7.33 (m, 10H), 4.18 (q, JH,H=7.1 Hz, 4H), 2.80 (s, 6H), 1.08 ppm (t, JH,H=7.1 Hz, 6H); $^{13}$C NMR (75 MHz, $CDCl_3$): d 163.64, 154.18, 146.81, 139.98, 131.22, 130.26, 129.29, 128.29, 122.91, 119.72, 60.47, 14.34, 13.87 ppm; HRMS (APCI positive) calcd for $[M+H]^+$:606.2316, found 606.2431.

**Synthesis of 4: 3** (3.6 g, 5.94 mmol) was dissolved in dry $CH_2Cl_2$ (40 mL). Then KCN (8.9 mmol, 580 mg) and 18-crown-6 ether (11.88 mmol, 3.13 g) were added to the solution. The resulting mixture was stirred for 30 min until fluorescence disappeared and the solution became colorless. Then hexane (80 mL) was added to the solution and left overnight. After 12 h the solution was decanted and the resulting white oil was washed with hexane, and dried to give 2.99 g (yield 80%) of pale gray crystals of compound **4**. $^1$H NMR (300 MHz, [$D_6$] DMSO): d 7.46–7.20 (m, 11H), 5.30 (s, 1H), 4.07–3.96 (m, 4H), 3.55 (s, 24H), 2.56 (s, 3H), 2.52 (s, 3H) 1.03–0.95 ppm (m, 6H); $^{13}$C NMR (75 MHz, $CDCl_3$): 164.63, 163.96, 134.43, 133.11, 132.98, 130.05, 129.52, 127.85, 127.80, 127.39, 126.56, 69.45, 59.18, 58.54, 30.92, 22.03, 13.80, 13.71 ppm.

Attempted preparation of **5**: Bromine (5.72 mmol, 0.3 mL) was added dropwise to a solution of (**4)** (1.3 g, 1.43 mmol) in THF (20 mL). The resulting mixture was stirred for 20 min at room temperature. Then the solution was poured into ice water (40 mL) and stirred for 30 min. Then the resulting precipitate was filtered and dried. The crude product was purified by column chromatography on silica gel using $CH_2Cl_2$ as the eluent to give 398 mg (yield 47%) of compound 3 and 442 mg (Yield 53%) of **6. (6)**: $^1$H NMR (300 MHz, CDCl3): d 11.09 (s, 1H), 7.71 (s, 1H), 7.49–7.30 (m, 10H), 4.17 (q, JH,H=7.1 Hz, 2H), 4.07 (q, JH,H=7.1 Hz, 2H), 2.75 (s, 3H), 2.71 (s, 3H), 1.07 (t, JH,H=7.1 Hz, 3H), 0.95 ppm (t, JH,H=7.1 Hz, 3H); $^{13}$C NMR (75 MHz, $CDCl_3$): d 164.29, 163.16, 149.95, 148.64, 143.45, 137.86, 132.76, 130.98, 130.48, 129.46, 128.64, 128.31, 127.70, 122.83, 117.07, 112.86, 60.66, 59.92, 15.57, 13.93, 13.81 ppm; HRMS (APCI positive) calcd for $[M+H]^+$: 584.2281, found 584.2448.

**Synthesis of compounds 7** and **8**: A mixture of (**3**) (400 mg, 0.66 mmol), ferrocene carboxaldehyde (353 mg, 1.65 mmol), piperidine (280 mg, 3.3 mmol), and acetic acid (396 mg, 6.6 mmol) in dry toluene (20 mL) was refluxed for 5 h. After cooling to room temperature, the solution was washed with water, and the organic layer was dried over $Na_2SO_4$, then evaporated to dryness. The crude product was purified by column chromatography on silica gel using $CH_2Cl_2$ as an eluent to give a mixture of **7** (138.6 mg, yield 21%) and **8** (63.6 mg, yield 12%).

Compound **7:** $^1$H NMR (300 MHz, $CDCl_3$): d 7.91 (s, 1H), 7.84 (s, 1H), 7.59 (d, $J_{HH}$ = 16.3 Hz, 1H), 7.54–7.35 (m, 11H), 4.57 (t, $J_{HH}$ = 1.8 Hz, 2H), 4.44 (t, $J_{HH}$ =1.8 Hz, 2H), 4.20 (s, 5H), 4.18–4.11(m, 4H), 2.80 (s, 3H), 1.08 (t, $J_{HH}$ = 7.1, 3H), 1.04 ppm (t, J=7.16 Hz, 3H); $^{13}$C NMR (75 MHz, $CDCl_3$): d 164.43, 163.72, 150.02, 146.69, 142.20, 139.13, 138.18, 131.52, 131.26, 130.32, 129.94, 129.25, 129.12, 128.54, 128.27, 123.69, 122.87, 120.68, 119.59, 81.60, 71.09, 70.01, 68.50, 61.09, 60.47, 29.85, 14.32, 13.97, 13.87 ppm; HRMS (APCI positive) calcd for $[M+H]^+$: 803.2295, found 803.2529.

Compound **8**: $^1$H NMR (300 MHz, $CDCl_3$): d 7.90 (s, 2H), 7.59 (d, $J_{HH}$ =16.3 Hz, 2H), 7.49–7.39 (m, 10H), 7.28 (d, $J_{HH}$ =16.3 Hz, 2H), 4.58 (t, $J_{HH}$=1.8 Hz, 4H), 4.43 (t, JH,H=1.8 Hz, 4H), 4.21 (s, 10H), 4.16 (q, $J_{HH}$=7.1 Hz, 4H), 1.04 ppm (t, $J_{HH}$=7.1 Hz, 6H); $^{13}$C NMR (75 MHz, $CDCl_3$): d 164.62, 153.37, 149.48, 145.97, 141.68, 137.49, 131.48, 130.01, 129.15, 128.53, 123.78, 120.55, 113.35, 109.47, 81.74, 70.98, 69.98, 68.43, 60.96, 13.98 ppm; HRMS (APCI positive) calcd for $[M+H]^+$: 999.2275, found 999.2582.

**Synthesis of 9**: A mixture of **8** (50 mg, 0.05 mmol), potassium cyanide (5 mg, 0.075 mmol), and 18-crown-6 (20 mg, 0.075 mmol) in dry $CH_2Cl_2$ (15 mL) was stirred at room temperature until the initially dark purple solution changed into a light orange solution. Then the unreacted precipitate was filtered off and solution was evaporated to dryness. The resulting precipitate was washed with hexane and dried yielding 40 mg (60%) of salt **9**. $^1$H NMR (300 MHz, $CDCl_3$): d 7.64 (s, 1H), 7.38–7.30 (m, 12H), 7.00– 6.94 (m, 1H), 5.78 (s, 1H), 4.48 (t, $J_{HH}$ =1.5 Hz, 2H), 4.45 (t, $J_{HH}$ = 1.5 Hz, 2H), 4.25 (t, $J_{HH}$ =1.5 Hz, 2H), 4.22 (t, $J_{HH}$ =1.5 Hz, 2H), 4.17 (s, 5H), 4.16 (s, 5H), 4.12–4.05 (m, 4H), 3.53 (s, 24H), 1.02 ppm (t, $J_{HH}$ =7.1 Hz, 6H); $^{13}$C NMR (75 MHz, $CDCl_3$): d 166.45, 134.89, 133.83, 130.11, 128.25, 127.45, 126.65, 119.45, 116.90, 115.76, 84.23, 83.74, 70.35, 69.63, 69.47, 69.35, 68.92, 67.33, 67.30, 67.11, 67.00, 60.24, 59.75, 34.83, 25.46, 14.10, 13.97 ppm.

Attempted preparation of **10**: To a solution of compound **14** (25 mg, 0.019 mmol) in dry $CH_2Cl_2$ (5 mL) tris(4-bromophenyl)aminium hexachloridoantimonate (Magic Blue) (15.4 mg, 0.019 mmol) was added and the resulting mixture was stirred for one minute. Then the solution was filtered and triethylamine (1 mL) was added. The organic layer was washed with water, dried ($Na_2SO_4$), and evaporated to dryness. The resulting crude product was purified by flash chromatography on silica gel using $CH_2Cl_2$ as a solvent yielding starting material **8**. No traces of the desired **10** were detected either by TLC or UV/Vis spectroscopy. Due to the salt **9** returning to **8** upon oxidation, several experiments of the same procedure with varying oxidants of different strengths were

undertaken. Reaction progress was monitored with UV/Vis absorption, and the formation of **8** were observed in all cases.

**Electrochemistry and Spectroelectrochemistry:**

The reduction/oxidation properties were also used to characterize the new BOPHY (**2)** using cyclic voltammetry (CV) and differential pulse voltammetry (DPV) electrochemical methods. The redox properties were referenced to $Fc/Fc^+$ with tetrabutylammonium tetarkis(pentafluorophenyl)borate (TBAF).

The spectroelectrochemistry experiments were carried out on the ferrocene BOPHYs (**2**, **7,** and **8**) in a custom 1 mm cell with a platinum mech working electrode, a platinum auxiliary, and a Ag/AgCl reference electrode. TBAF (0.15 M) in DCM was used as an electrolyte. Chemical titrations were carried out in a 10 mm cuvette with 0.01 M iron (III) perchlorate additions. UV-Vis data was collected on a Jasco-720 spectrophotometer.

**Computational Details**

All calculations were performed using Gaussian 09 under Unix OS at the University of Minnesota Supercomputing Institute (MSI). In order to model the system more accurately $C_i$ and $C_2$ symmetries were optimized. The TPSSh hybrid exchange-correlation functional, the 6-311+G basis set was used for iron atoms, and 6-311G(d) basis set was used for all over atoms. Using the PCM approach with dichloromethane as a solvent, calculations ensured solvent like conditions. Frequencies were calculated to ensure all geometries were represent and energy minima on the potential energy surface. PCM-TDDFT calculations, the first 50 excited states were accounted for.

## References


(1) Tamgho, I.-S.; Hasheminasab, A.; Engle, J. T.; Nemykin, V. N.; Ziegler, C. J. A New Highly Fluorescent and Symmetric Pyrrole–BF2 Chromophore: BOPHY. *J. Am. Chem. Soc.* **2014**, *136* (15), 5623–5626. https://doi.org/10.1021/ja502477a.

(2) Ulrich, G.; Ziessel, R.; Harriman, A. The Chemistry of Fluorescent Bodipy Dyes: Versatility Unsurpassed. *Angew. Chem. Int. Ed. Engl.* **2008**, *47* (7), 1184–1201. https://doi.org/10.1002/anie.200702070.

(3) Ziessel, R.; Ulrich, G.; Harriman, A. The Chemistry of Bodipy: A New El Dorado for Fluorescence Tools. *New J. Chem.* **2007**, *31* (4), 496–501. https://doi.org/10.1039/B617972J.

(4) Bochkov, A. Y.; Akchurin, I. O.; Dyachenko, O. A.; Traven, V. F. NIR-Fluorescent Coumarin-Fused BODIPY Dyes with Large Stokes Shifts. *Chem. Commun.* **2013**, *49* (99), 11653–11655. https://doi.org/10.1039/C3CC46498A.

(5) Boens, N.; Leen, V.; Dehaen, W. Fluorescent Indicators Based on BODIPY. *Chem. Soc. Rev.* **2012**, *41* (3), 1130–1172. https://doi.org/10.1039/C1CS15132K.

(6) Loudet, A.; Burgess, K. BODIPY Dyes and Their Derivatives: Syntheses and Spectroscopic Properties. *Chem. Rev.* **2007**, *107* (11), 4891–4932. https://doi.org/10.1021/cr078381n.

(7) Aza-BODIPY Derivatives: Enhanced Quantum Yields of Triplet Excited States and the Generation of Singlet Oxygen and their Role as Facile Sustainable Photooxygenation Catalysts - Adarsh - 2012 - Chemistry – A European Journal - Wiley Online Library https://onlinelibrary.wiley.com/doi/abs/10.1002/chem.201202438 (accessed Mar 28, 2019).

(8) Mishra, A.; Fischer, M. K. R.; Bäuerle, P. Metal-Free Organic Dyes for Dye-Sensitized Solar Cells: From Structure: Property Relationships to Design Rules. *Angew. Chem. Int. Ed. Engl.* **2009**, *48* (14), 2474–2499. https://doi.org/10.1002/anie.200804709.

(9) Gonçalves, M. S. T. Fluorescent Labeling of Biomolecules with Organic Probes. *Chem. Rev.* **2009**, *109* (1), 190–212. https://doi.org/10.1021/cr0783840.

(10) Han, J.; Burgess, K. Fluorescent Indicators for Intracellular PH. *Chem. Rev.* **2010**, *110* (5), 2709–2728. https://doi.org/10.1021/cr900249z.

(11) Dye-Sensitized Solar Cells - Chemical Reviews (ACS Publications) https://pubs.acs.org/doi/abs/10.1021/cr900356p (accessed Mar 28, 2019).

(12) Zheng, H.; Zhan, X.-Q.; Bian, Q.-N.; Zhang, X.-J. Advances in Modifying Fluorescein and Rhodamine Fluorophores as Fluorescent Chemosensors. *Chem. Commun.* **2012**, *49* (5), 429–447. https://doi.org/10.1039/C2CC35997A.

(13) Vendrell, M.; Zhai, D.; Er, J. C.; Chang, Y.-T. Combinatorial Strategies in Fluorescent Probe Development. *Chem. Rev.* **2012**, *112* (8), 4391–4420. https://doi.org/10.1021/cr200355j.

(14) Rhoda Hannah M.; Chanawanno Kullapa; King Alexander J.; Zatsikha Yuriy V.; Ziegler Christopher J.; Nemykin Victor N. Unusually Strong Long-Distance Metal–Metal Coupling in Bis(Ferrocene)-Containing BOPHY: An Introduction to Organometallic BOPHYs. *Chemistry – A European Journal* **2015**, *21* (50), 18043–18046. https://doi.org/10.1002/chem.201504004.

(15) Ziegler, C. J.; Chanawanno, K.; Hasheminsasab, A.; Zatsikha, Y. V.; Maligaspe, E.; Nemykin, V. N. Synthesis, Redox Properties, and Electronic Coupling in the Diferrocene Aza-Dipyrromethene and AzaBODIPY Donor-Acceptor Dyad with Direct Ferrocene-α-Pyrrole Bond. *Inorg Chem* **2014**, *53* (9), 4751–4755. https://doi.org/10.1021/ic500526k.

(16) Maligaspe, E.; Pundsack, T. J.; Albert, L. M.; Zatsikha, Y. V.; Solntsev, P. V.; Blank, D. A.; Nemykin, V. N. Synthesis and Charge-Transfer Dynamics in a Ferrocene-Containing Organoboryl Aza-BODIPY Donor-Acceptor Triad with Boron as the Hub. *Inorg Chem* **2015**, *54* (8), 4167–4174. https://doi.org/10.1021/acs.inorgchem.5b00494.

(17) Robin, M. B.; Day, P. Mixed Valence Chemistry-A Survey and Classification. In *Advances in Inorganic Chemistry and Radiochemistry*; Emeléus, H. J., Sharpe, A. G., Eds.; Academic Press, 1968; Vol. 10, pp 247–422. https://doi.org/10.1016/S0065-2792(08)60179-X.

(18) Didukh, N. O.; Zatsikha, Y. V.; Rohde, G. T.; Blesener, T. S.; Yakubovskyi, V. P.; Kovtun, Y. P.; Nemykin, V. N. NIR Absorbing Diferrocene-Containing Meso-Cyano-BODIPY with a UV-Vis-NIR Spectrum Remarkably Close to That of Magnesium Tetracyanotetraferrocenyltetraazaporphyrin. *Chem. Commun.* **2016**, *52* (77), 11563–11566. https://doi.org/10.1039/C6CC06344F.

(19) Maligaspe, E.; Hauwiller, M. R.; Zatsikha, Y. V.; Hinke, J. A.; Solntsev, P. V.; Blank, D. A.; Nemykin, V. N. Redox and Photoinduced Electron-Transfer Properties in Short Distance Organoboryl Ferrocene-Subphthalocyanine Dyads. *Inorg Chem* **2014**, *53* (17), 9336–9347. https://doi.org/10.1021/ic5014544.

(20) Zatsikha Yuriy V.; Nemez Dion B.; Davis Rebecca L.; Singh Simarpreet; Herbert David E.; King Alex J.; Ziegler Christopher J.; Nemykin Victor N. Testing the Limits of the BOPHY Platform: Preparation, Characterization, and Theoretical Modeling of BOPHYs and Organometallic BOPHYs with Electron-Withdrawing Groups at B-Pyrrolic and Bridging Positions. *Chemistry – A European Journal* **2017**, *23* (59), 14786–14796. https://doi.org/10.1002/chem.201702597.

(21) Obondi, C. O.; Lim, G. N.; Karr, P. A.; Nesterov, V. N.; D'Souza, F. Photoinduced Charge Separation in Wide-Band Capturing, Multi-Modular Bis(Donor

Styryl)BODIPY–Fullerene Systems. *Phys. Chem. Chem. Phys.* **2016**, *18* (27), 18187–18200. https://doi.org/10.1039/C6CP03479A.

(22) Yakubovskyi, V. P.; Didukh, N. O.; Zatsikha, Y. V.; Kovtun, Y. P. A New Approach to the Synthesis of Meso-CN-Substituted BODIPYs. *ChemistrySelect* **2016**, *1* (7), 1462–1466. https://doi.org/10.1002/slct.201600246.

(23) Bucher, L.; Aly, S. M.; Desbois, N.; Karsenti, P.-L.; Gros, C. P.; Harvey, P. D. Random Structural Modification of a Low-Band-Gap BODIPY-Based Polymer. *J. Phys. Chem. C* **2017**, *121* (12), 6478–6491. https://doi.org/10.1021/acs.jpcc.7b00117.

(24) Zatsikha, Y. V.; Maligaspe, E.; Purchel, A. A.; Didukh, N. O.; Wang, Y.; Kovtun, Y. P.; Blank, D. A.; Nemykin, V. N. Tuning Electronic Structure, Redox, and Photophysical Properties in Asymmetric NIR-Absorbing Organometallic BODIPYs. *Inorg. Chem.* **2015**, *54* (16), 7915–7928. https://doi.org/10.1021/acs.inorgchem.5b00992.

# Appendix A

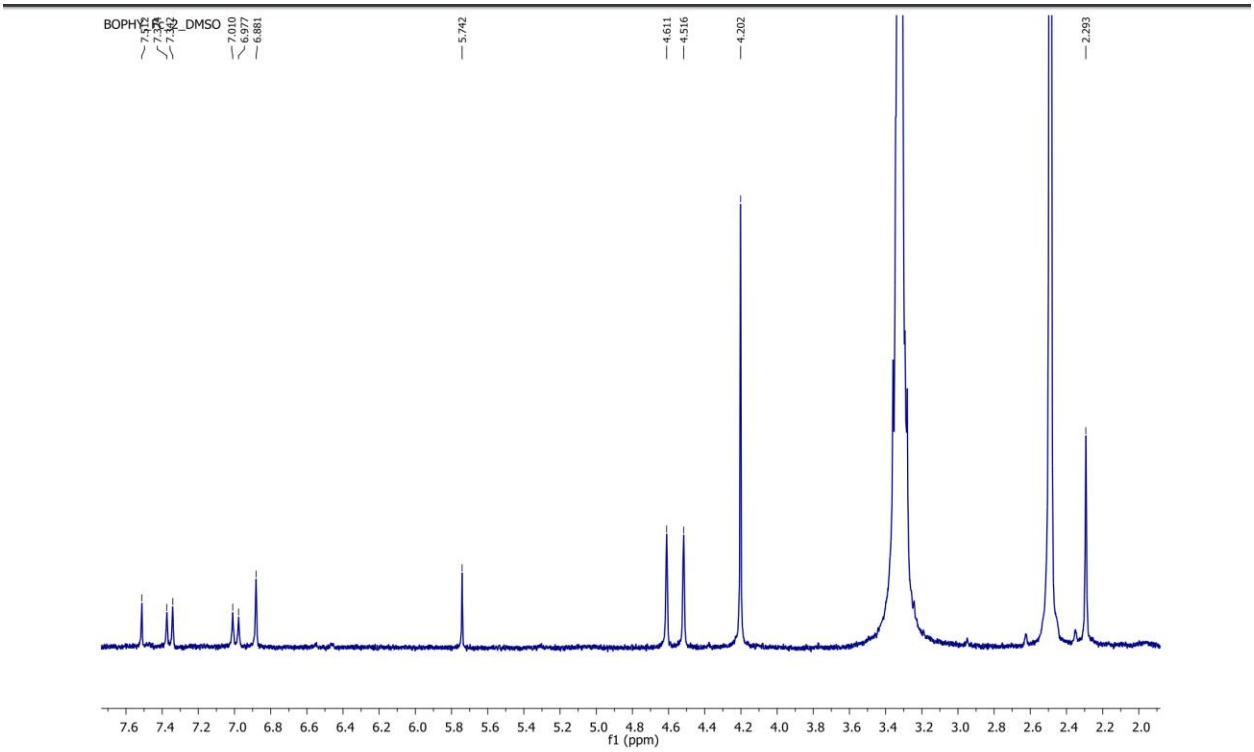


Figure A.1: $^{1}$H NMR (500 MHz) of bis(ferrocene)BOPHY (2)

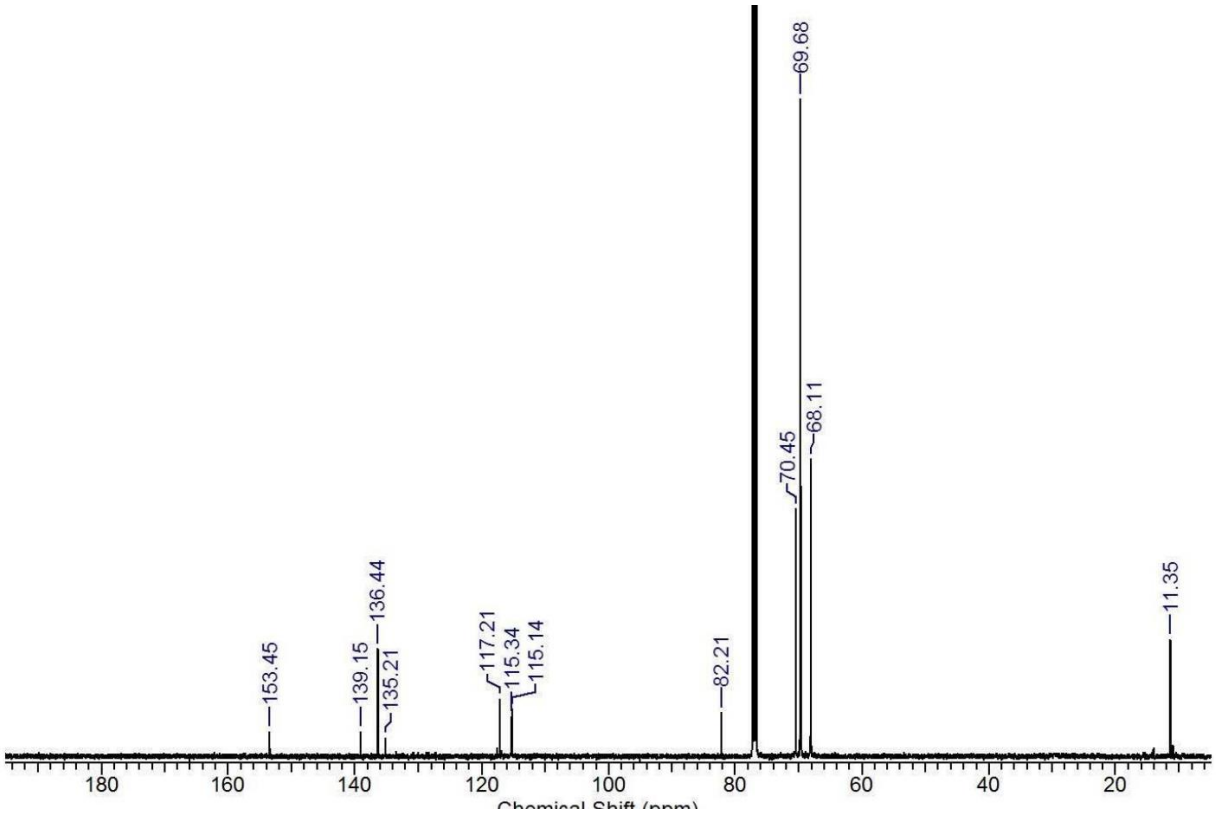


Figure A.2: $^{13}$C NMR of bis(ferrocene)BOPHY (2)

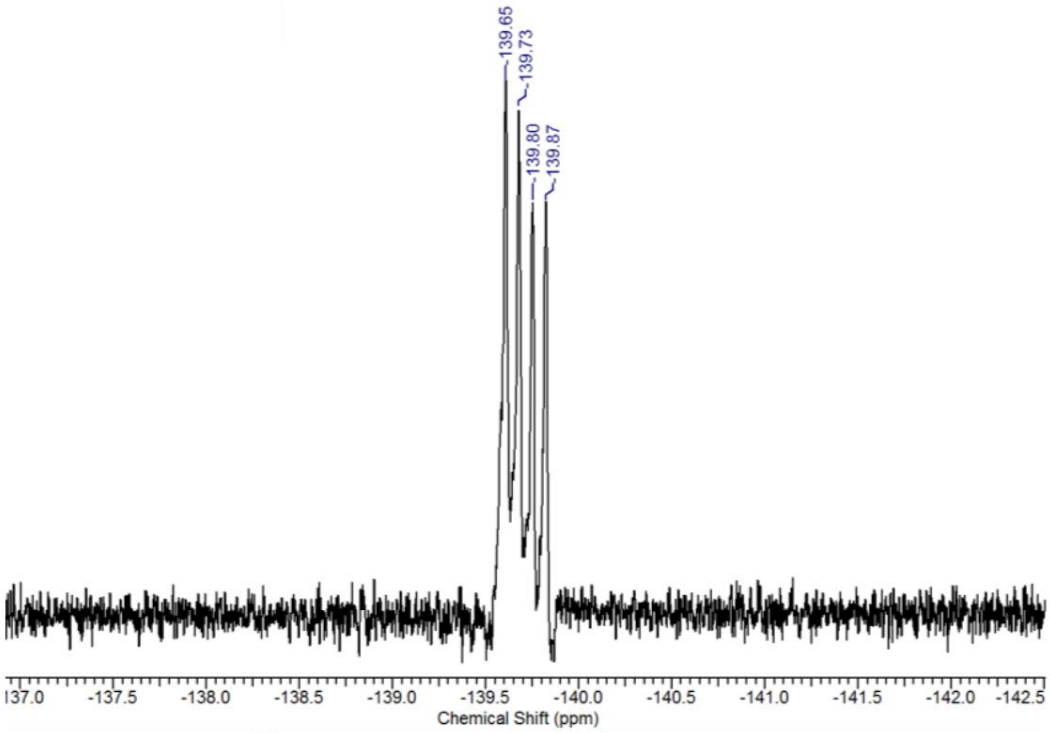


Figure A.3: $^{19}$F NMR of bis(ferrocene)BOPHY (2)

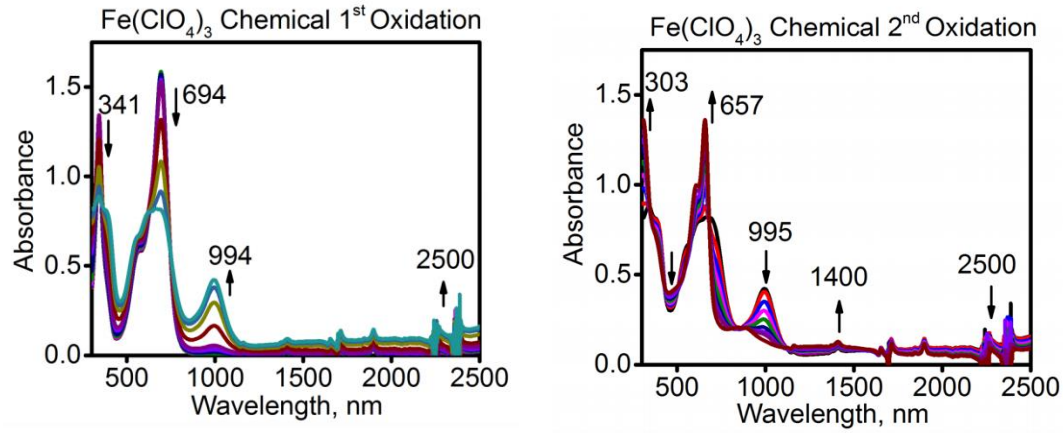


Figure A.4: First and second chemical oxidation by Iron (iii) perchlorate.

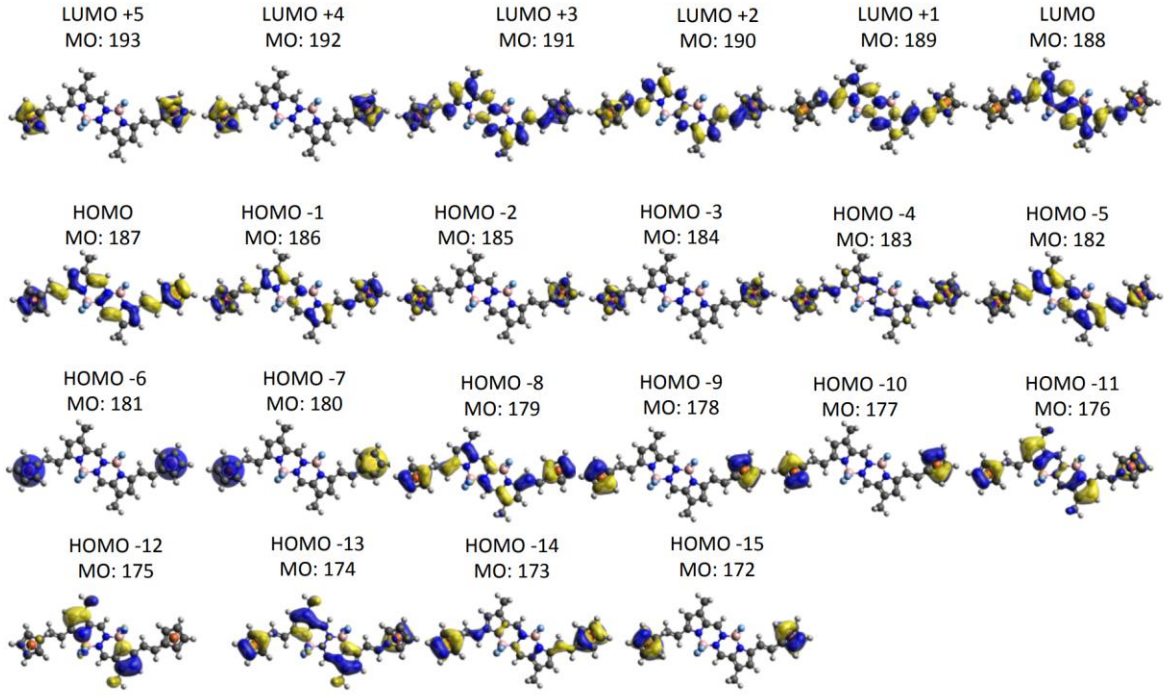


Figure A.5: MOs for $C_i$ symmetry

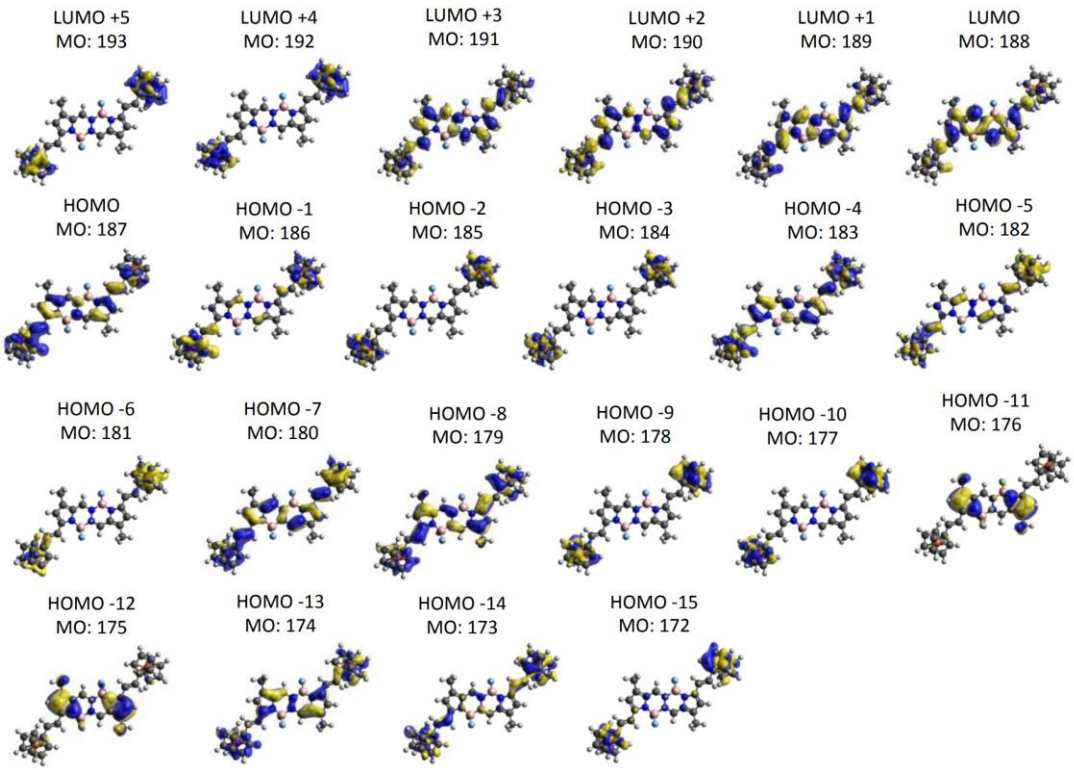


Figure A.6: MOs for $C_2$ symmetry.

Table A.1: Electronic density distribution for C2 Symmetry of Bis(fc)-BOPHY (2)

| | | | % MO Composition | | | | |
|---|---|---|---|---|---|---|---|
| MO | Energy (eV) | Symmetry | N-N Bridge | BF2 | BOPHY | Fe | Cp |
| | | | **$C_2$ Symmetry** | | | | |
| 182 | -5.707 | A | 2.52 | 0.28 | 21.51 | 58.93 | 16.76 |
| 183 | -5.355 | B | 9.53 | 0.91 | 28.61 | 33.4 | 27.55 |
| 184 | -5.123 | A | 0 | 0 | 0.43 | 67.6 | 31.97 |
| 185 | -5.123 | B | 0 | 0 | 0.44 | 67.6 | 31.96 |
| 186 | -5.058 | A | 0.87 | 0.14 | 8.43 | 58 | 32.56 |
| **187** | **-4.886** | **B** | **8.73** | **0.71** | **28.74** | **39.2** | **22.62** |
| **188** | **-2.973** | **A** | **7.4** | **1.41** | **79.2** | **5.5** | **6.48** |
| 189 | -2.079 | B | 20.87 | 1.08 | 60.21 | 7.51 | 10.33 |
| 190 | -1.245 | A | 1.43 | 0.44 | 56.31 | 18.9 | 22.91 |
| 191 | -1.067 | B | 9.57 | 0.97 | 52.4 | 17.08 | 19.98 |
| 192 | -0.78 | A | 0 | 0 | 0.97 | 41.05 | 57.97 |
| 193 | -0.78 | B | 0.01 | 0 | 1.02 | 41.03 | 57.93 |

Table A.2: IVCT Band properties from deconvolution analysis

| Complex | $\nu$, $cm^{-1}$ | $\nu_{1/2}$, $cm^{-1}$ | $\varepsilon$, $M^{-1}$ $cm^{-1}$ | $H_{ab}$, $cm^{-1}$ | $\nu_{1/2}$, $cm^{-1}$ (theor.) | $R_{MM}$, Å | $\Gamma$ |
|---|---|---|---|---|---|---|---|
| $[2]^{+a}$ | 5431 | 3804 | 2247 | 258 | 3531 | 17.2 | 0.0773 |
| $[2]^{+b}$ | 5376 | 3532 | 2139 | 241 | 3513 | 17.2 | 0.0054 |

TDDFT excited states can be found in the supporting information for *Unusually Strong Long-Distance Metal–Metal Coupling in Bis(ferrocene)-Containing BOPHY: An Introduction to Organometallic BOPHYs.*[14]

## Appendix B:

NMR Spectra

Each compound was analyzed through proton and carbon NMR spectroscopy. Compounds are first listed with the $^{1}$HNMR spectrum followed by the $^{13}$CNMR spectrum. Solvents used are listed in the synthetic section above.

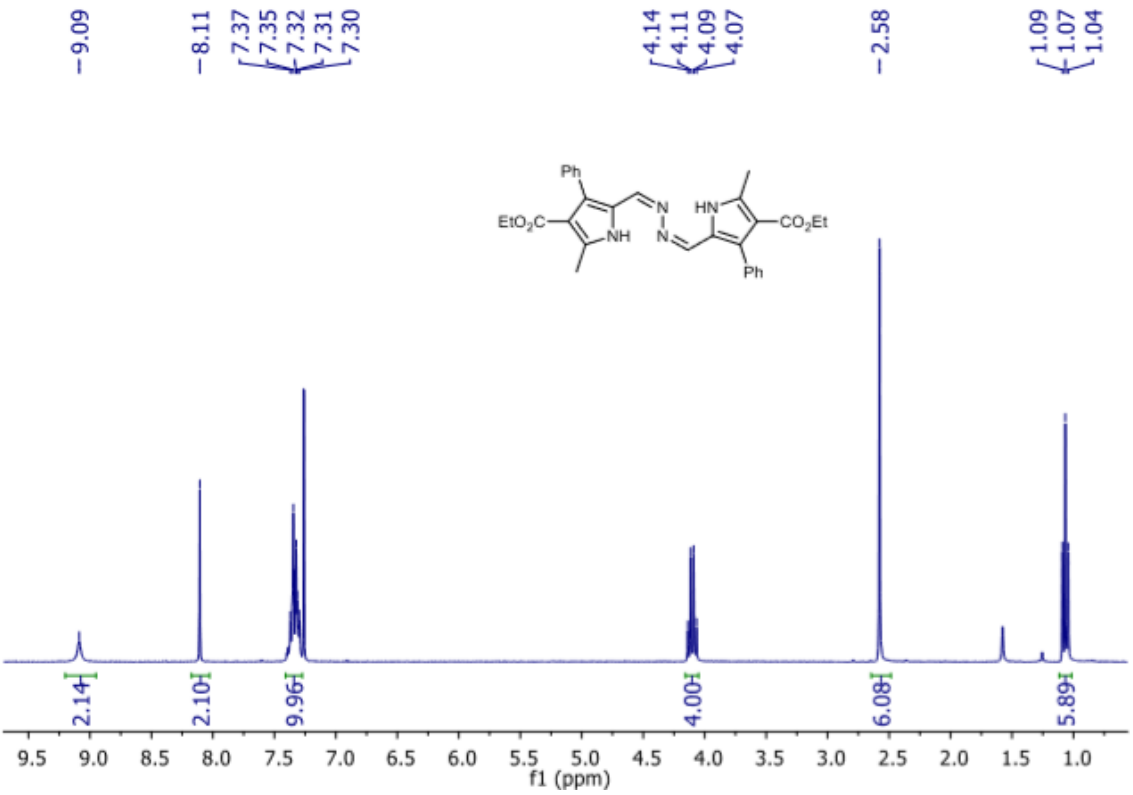


Figure B.1.1: $^{1}$H NMR of the Schiff-Base ligand **b**.

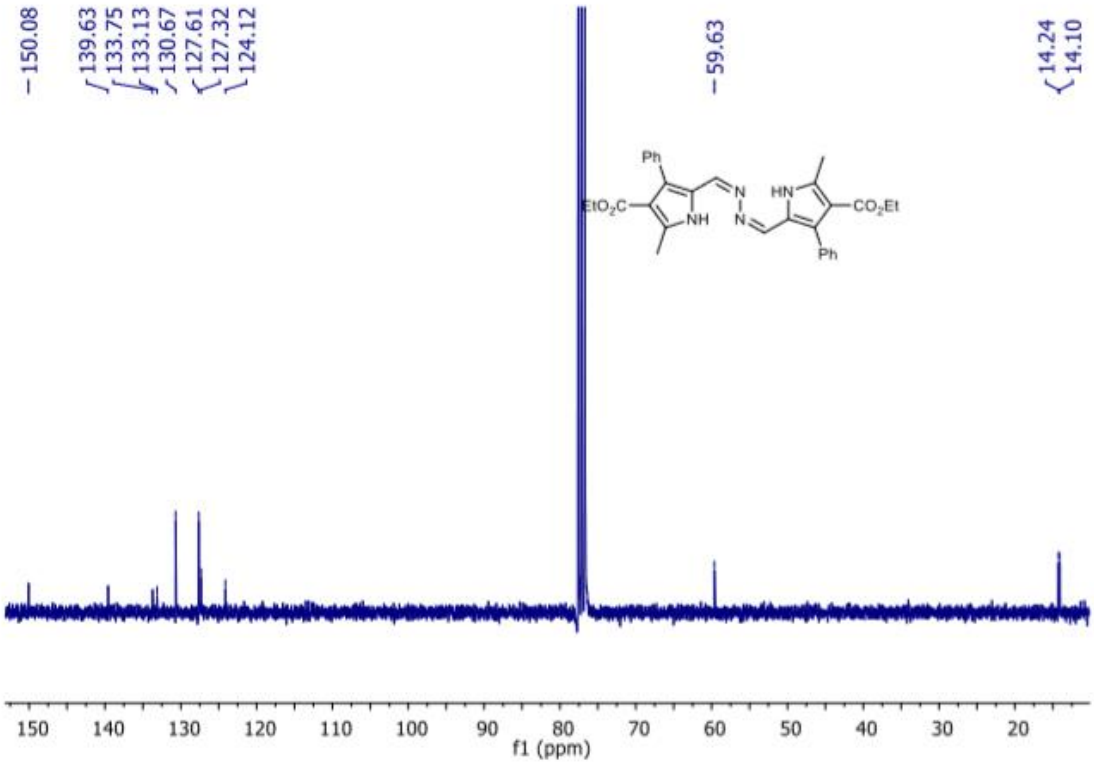

Figure B.1.2: $^{13}C$ NMR of the Schiff-Base ligand **b**.

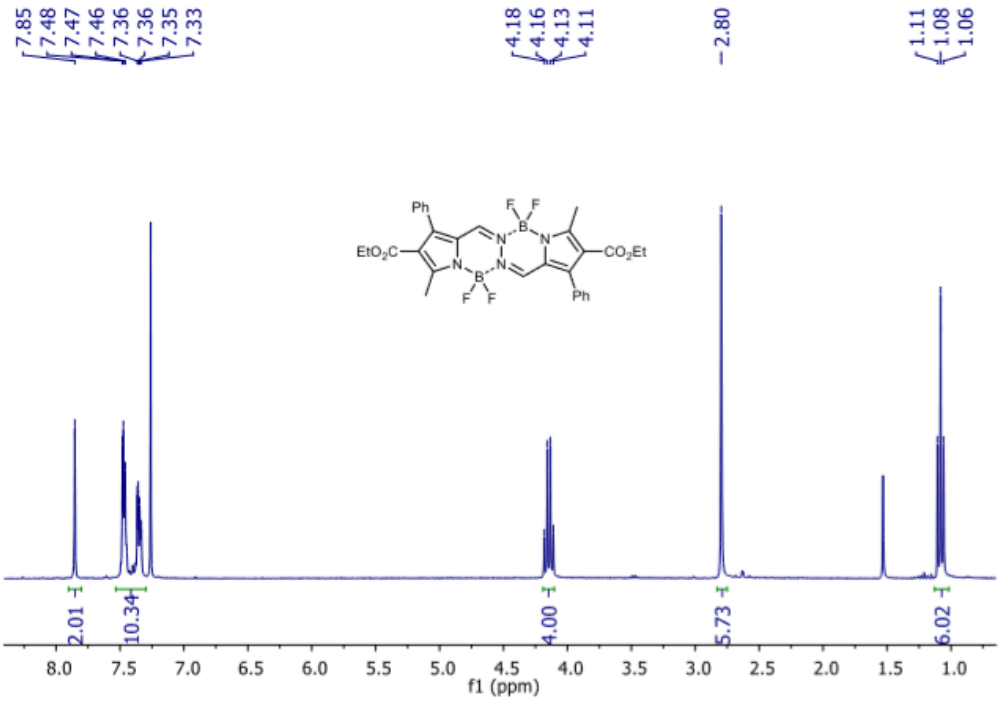

Figure B.1.3: $^{1}$H NMR of **3.**

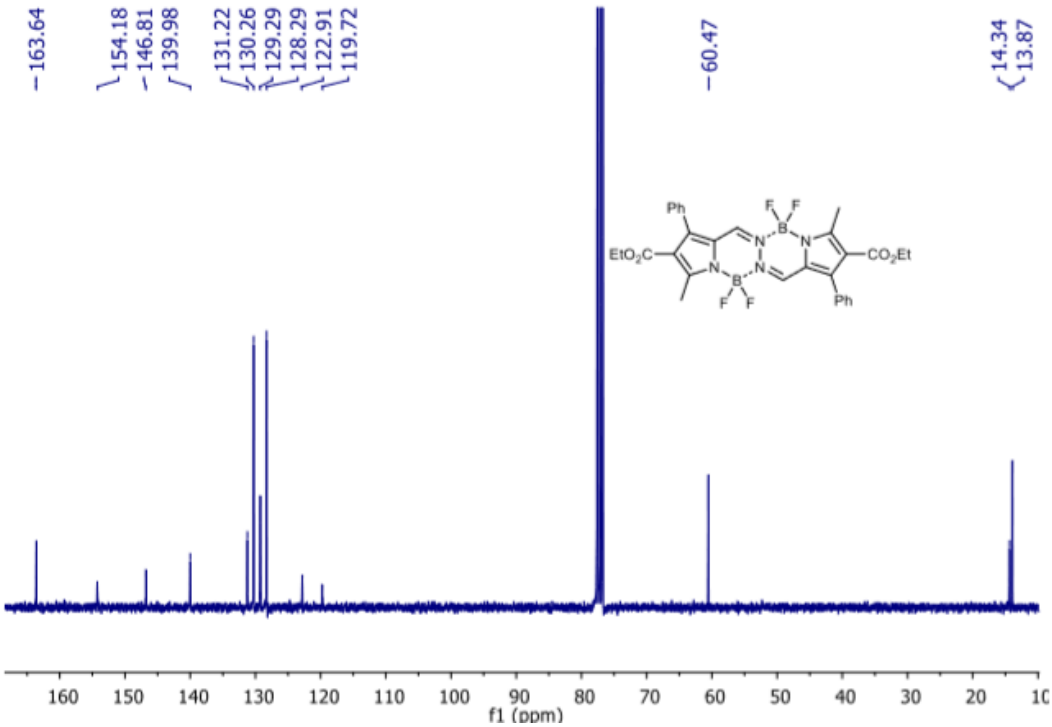


Figure B.1.4: $^{13}$C NMR of **3**

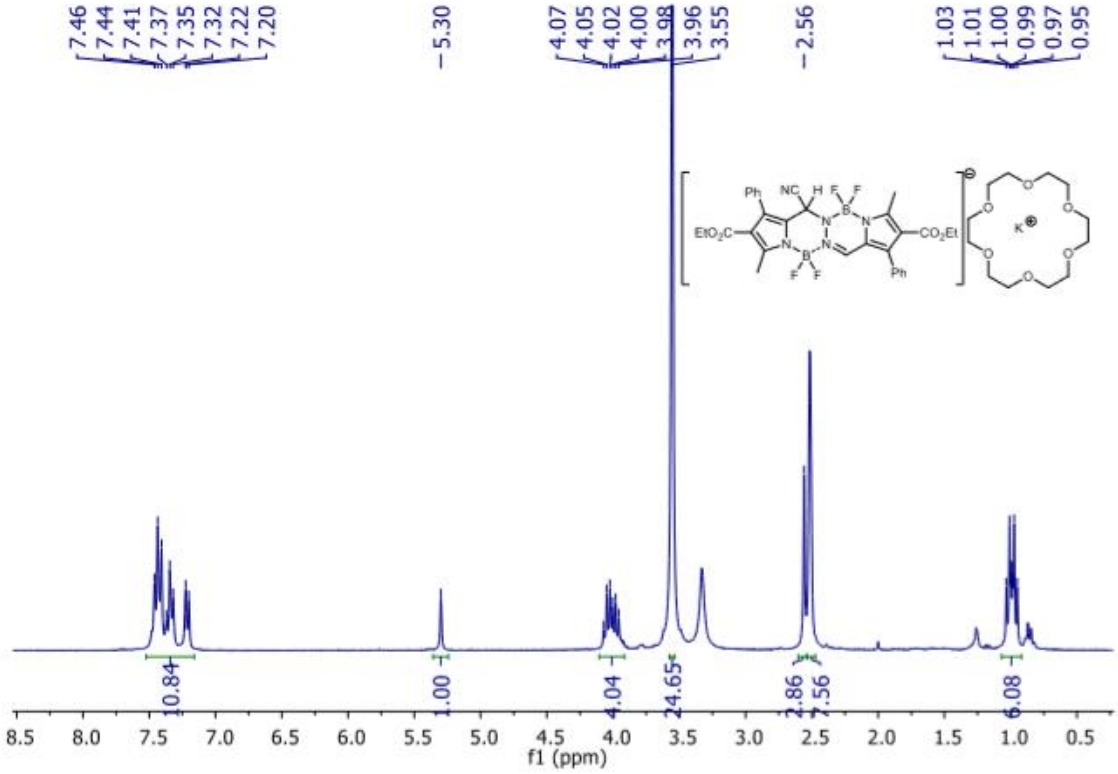
7.46
7.44
7.41
7.37
7.35
7.32
7.22
7.20
5.30
4.07
4.05
4.02
4.00
3.98
3.96
3.55
2.56
1.03
1.01
1.00
0.99
0.97
0.95
10.84
1.00
4.04
24.65
2.86
7.56
6.08
8.5 8.0 7.5 7.0 6.5 6.0 5.5 5.0 4.5 4.0 3.5 3.0 2.5 2.0 1.5 1.0 0.5
f1 (ppm)

Figure B.1.5: $^{1}$H NMR of **4**

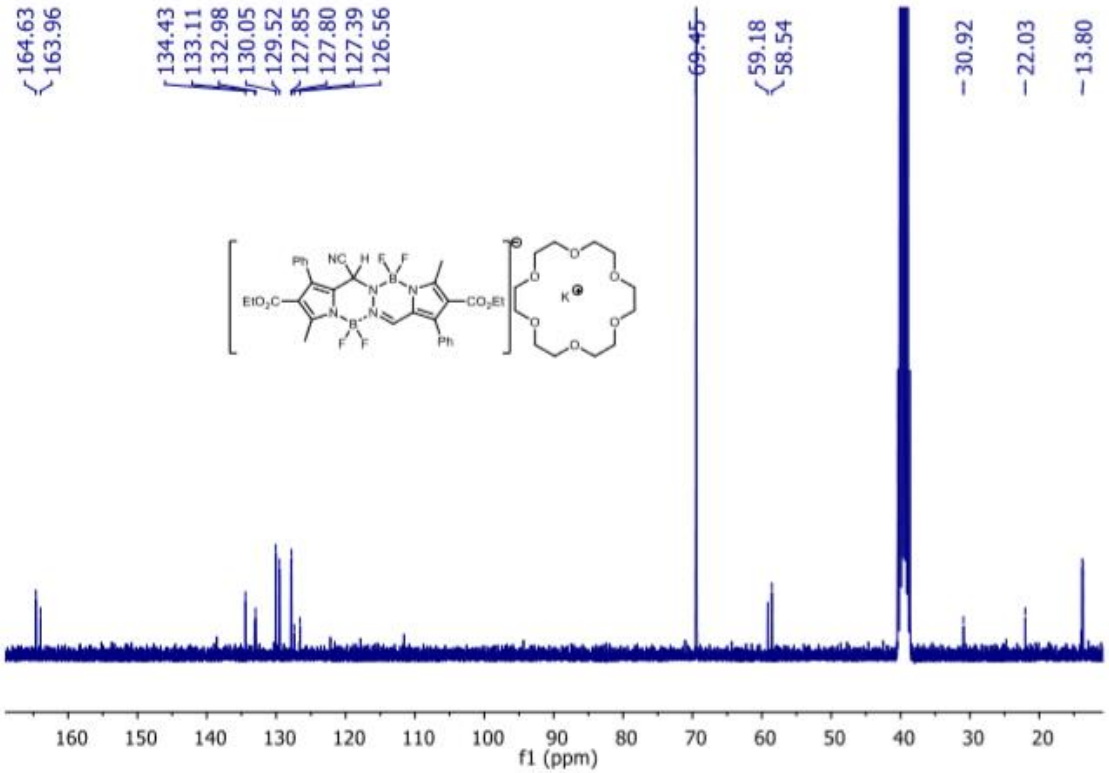


Figure B.1.6: $^{13}$C NMR of **4**

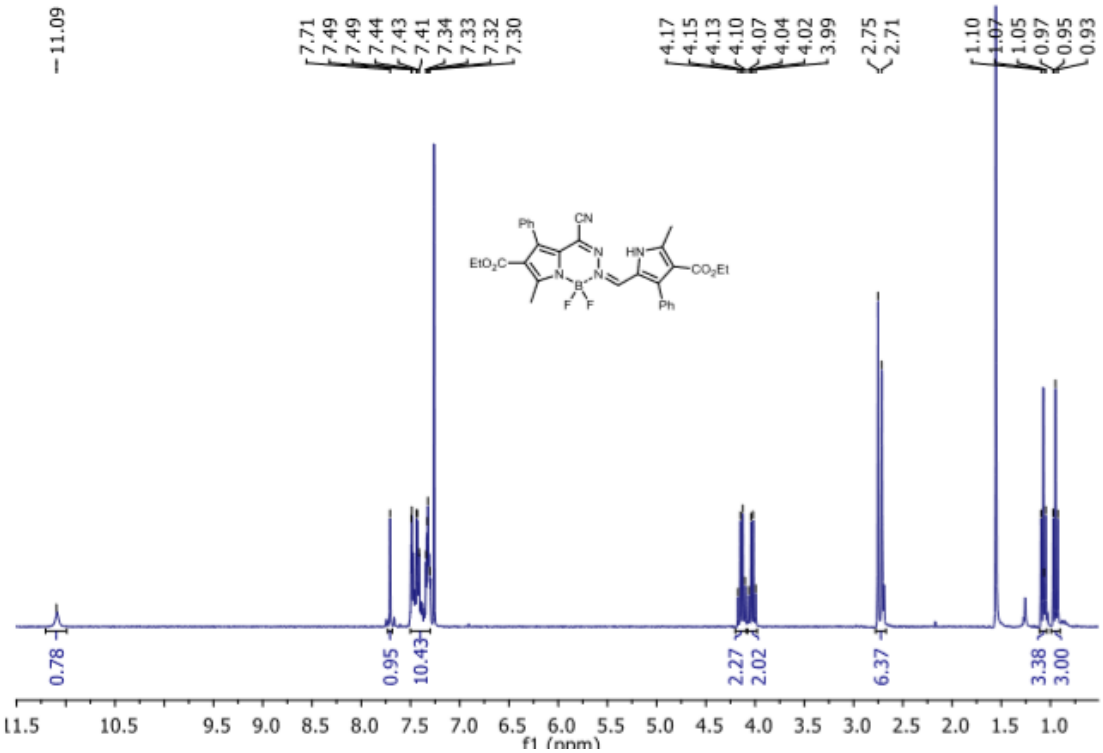


Figure B.1.7: $^{1}$H NMR of **6**

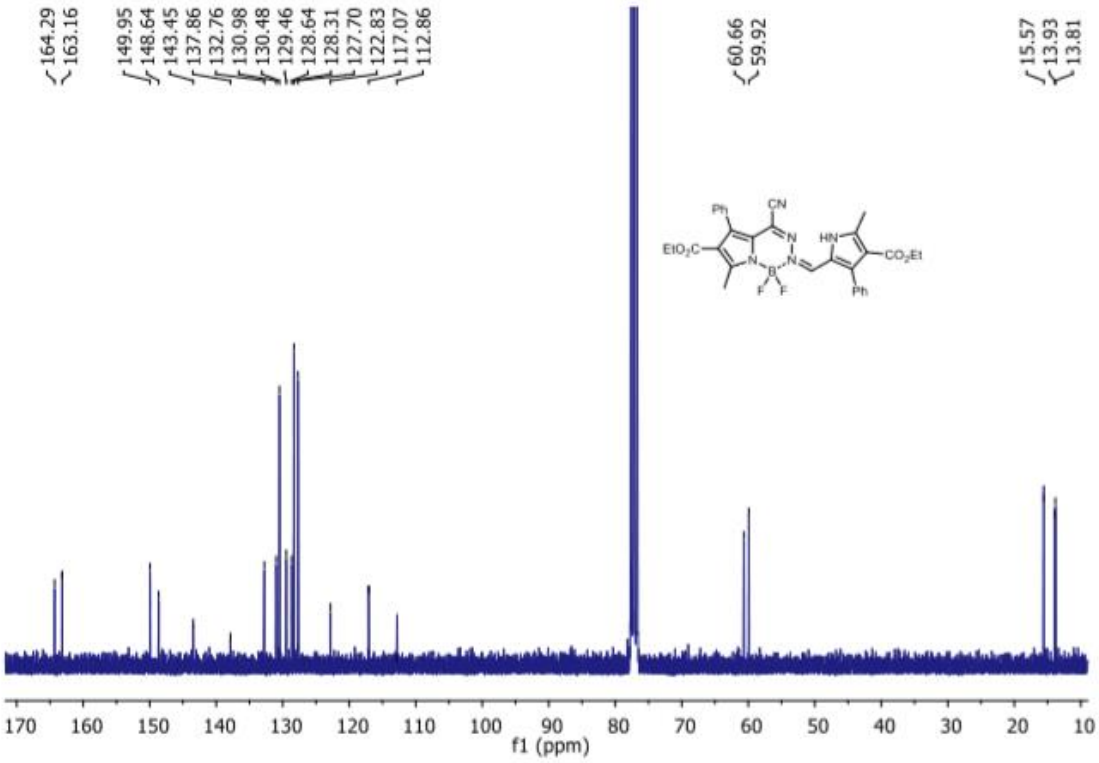

Figure B.1.8: $^{13}C$ NMR of **6**

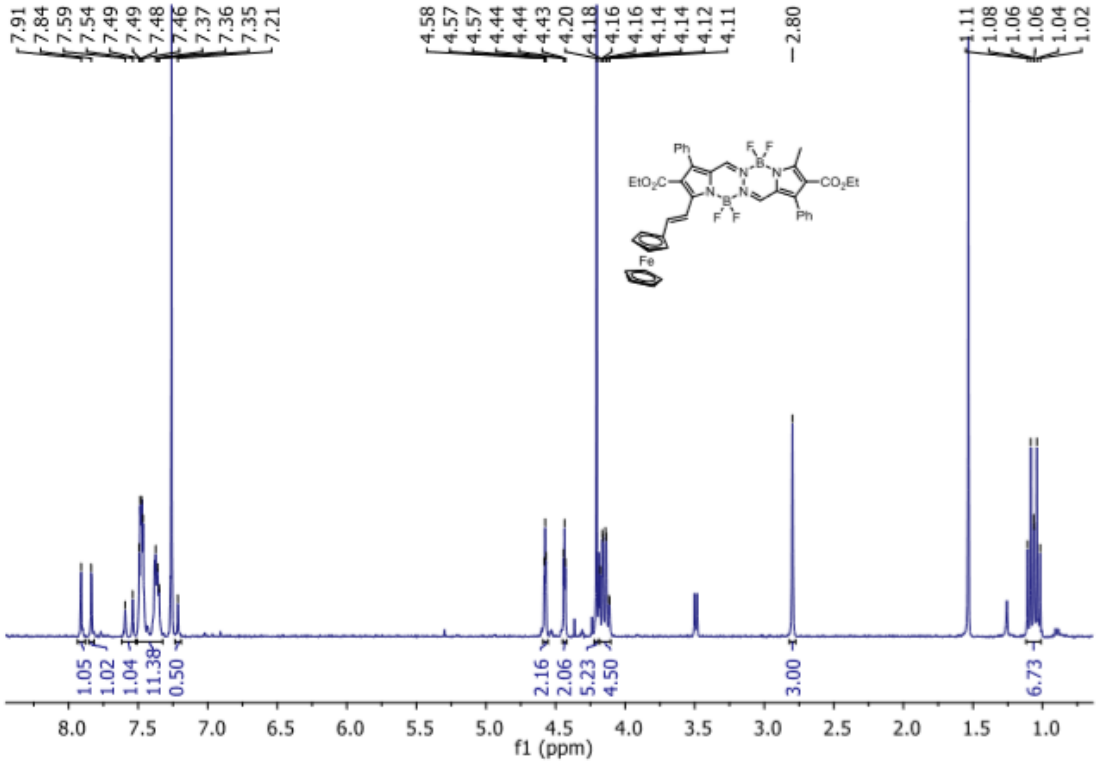


Figure B.1.9: $^{1}H$ NMR of **7**

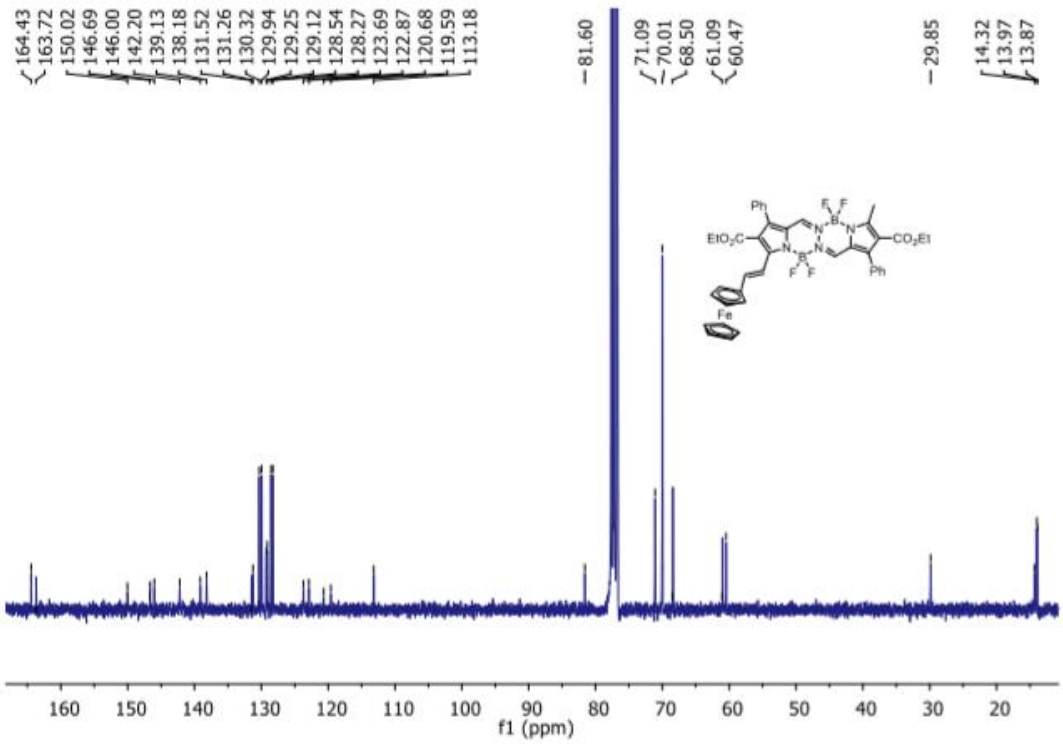


Figure B.1.10: $^{13}$C NMR of **7**

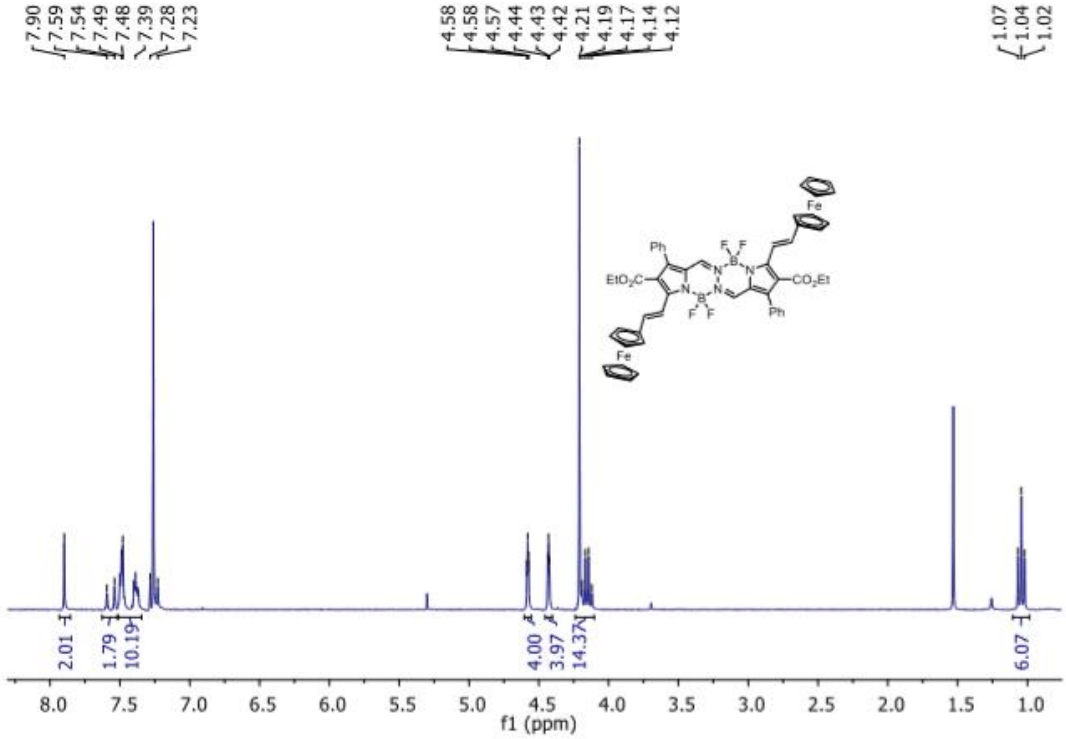


Figure B.1.11: $^{1}$H NMR of **8**

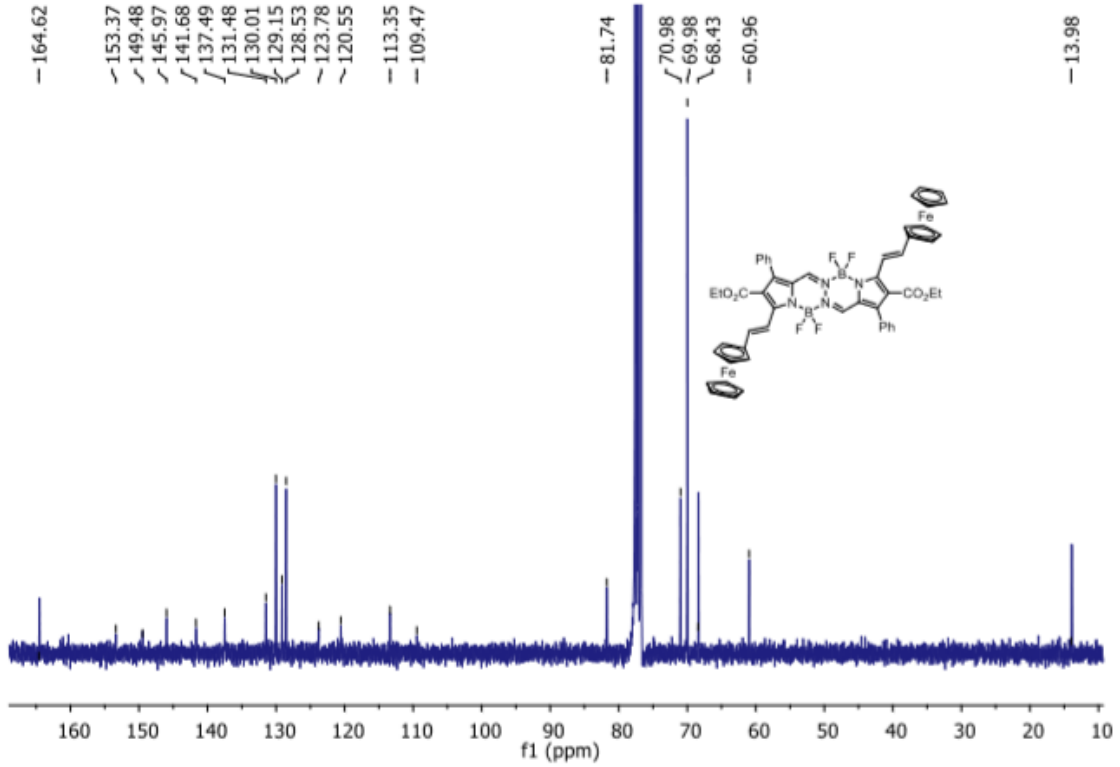


Figure B.1.12: $^{13}$C NMR of **8**

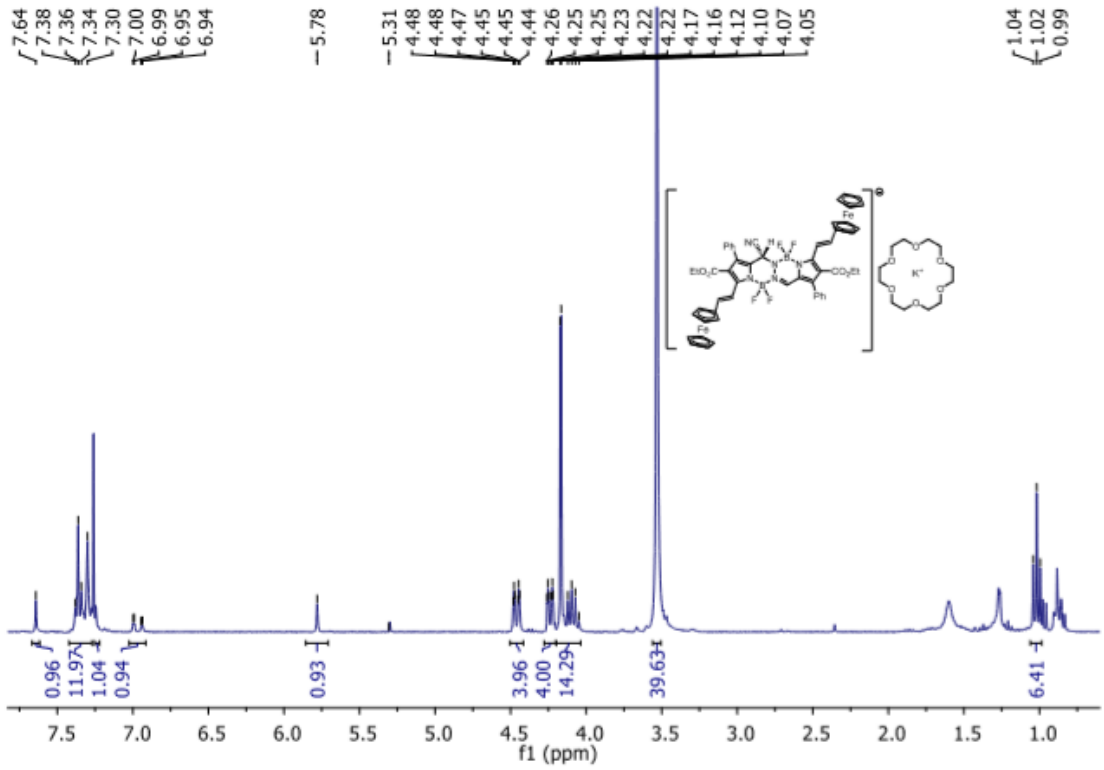

Figure B.1.13: $^{1}$H NMR of **9**

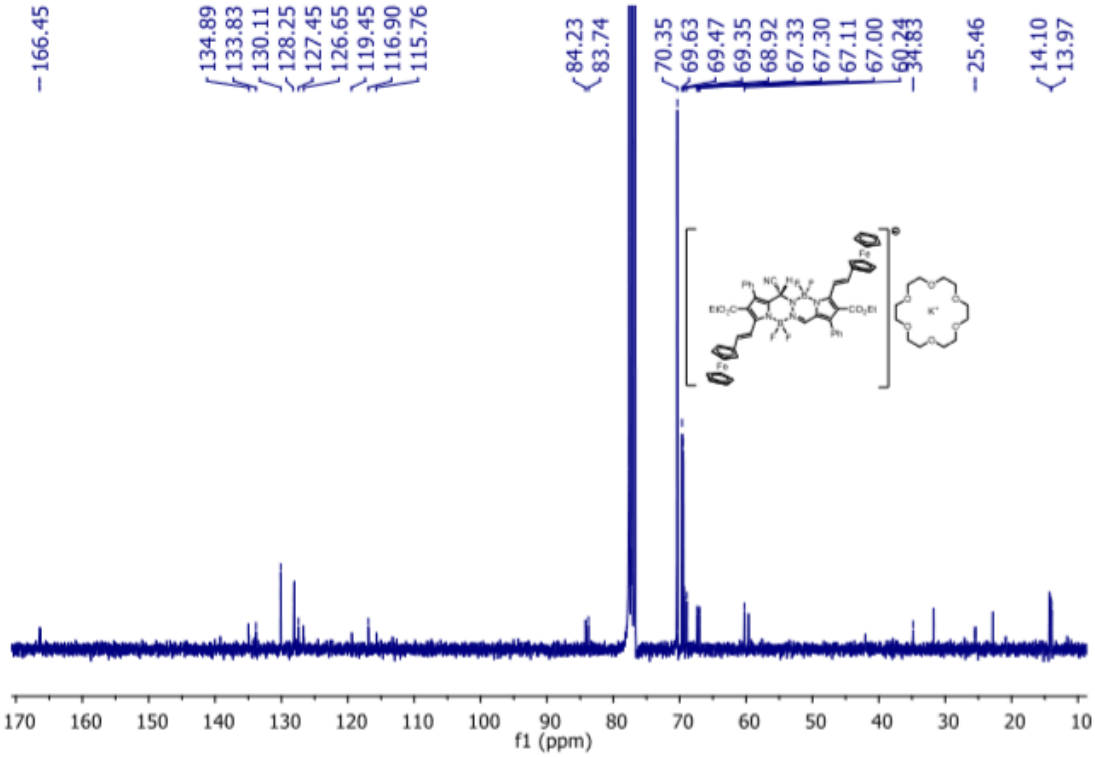


Figure B.1.14: $^{13}$C NMR of **9**

HRMS:

Compounds were analyzed using HRMS with either positive or negative APCI ionization methods (charge is specified in the synthesis section.

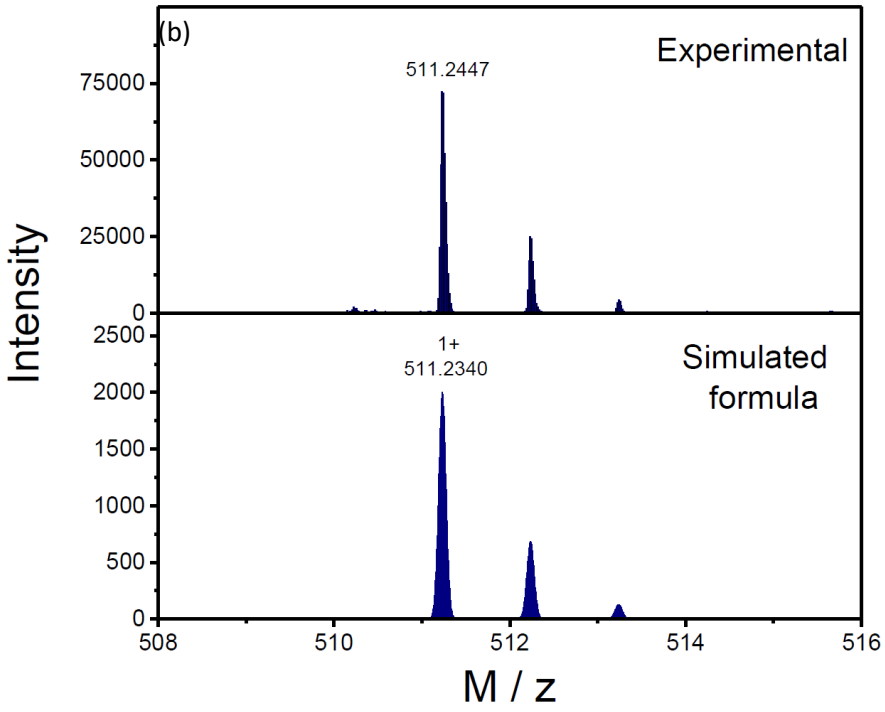
(b)
Experimental
511.2447
Simulated formula
1+
511.2340
Intensity
M / z

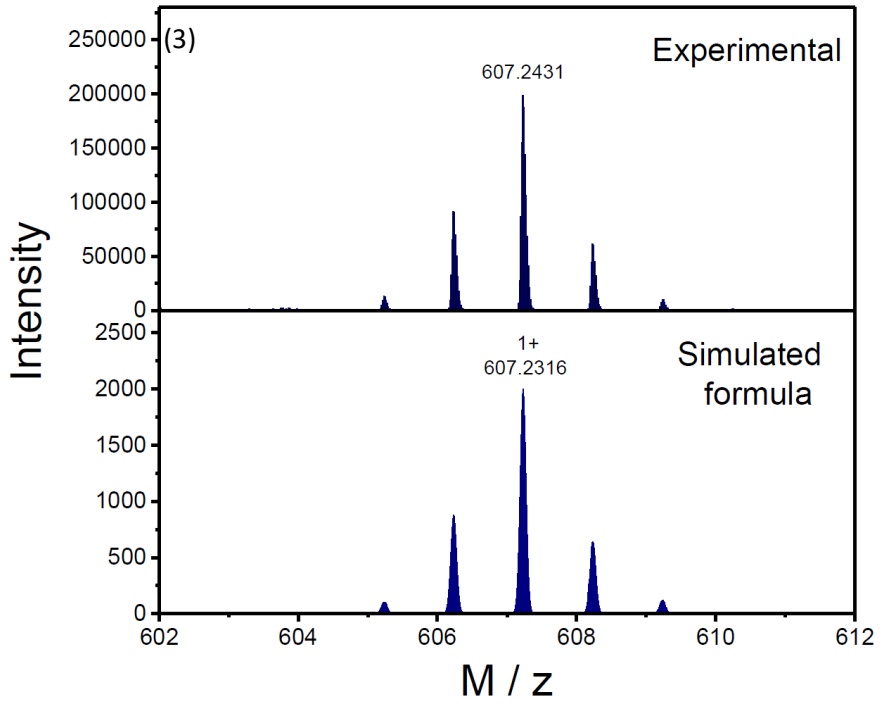
(3)
Experimental
607.2431
Simulated formula
1+
607.2316
Intensity
M / z

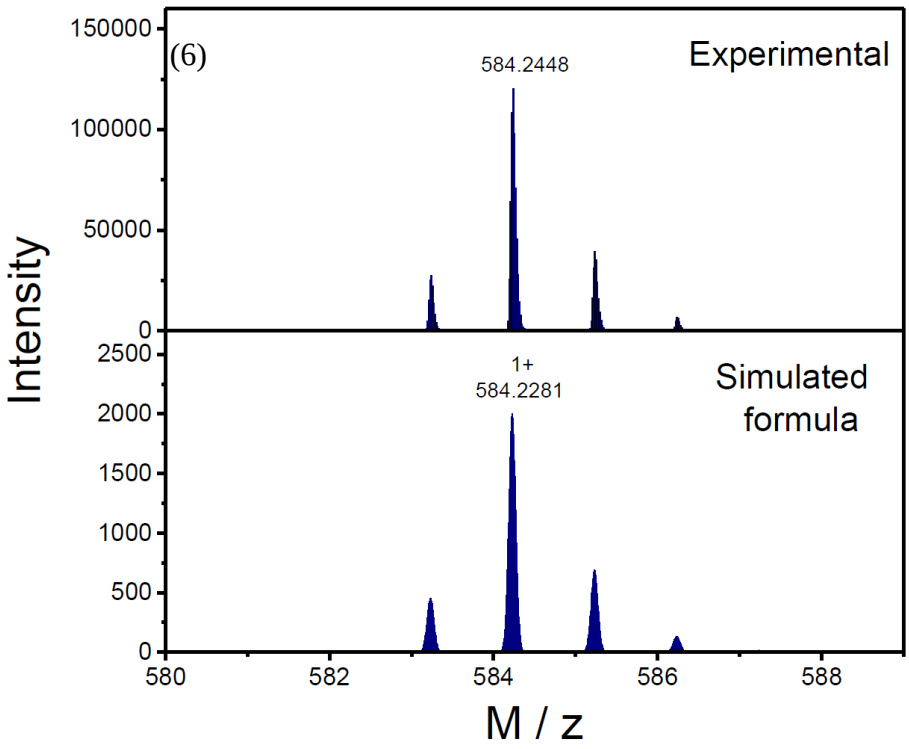
(6)
Experimental
584.2448
Simulated formula
1+
584.2281
Intensity
M / z

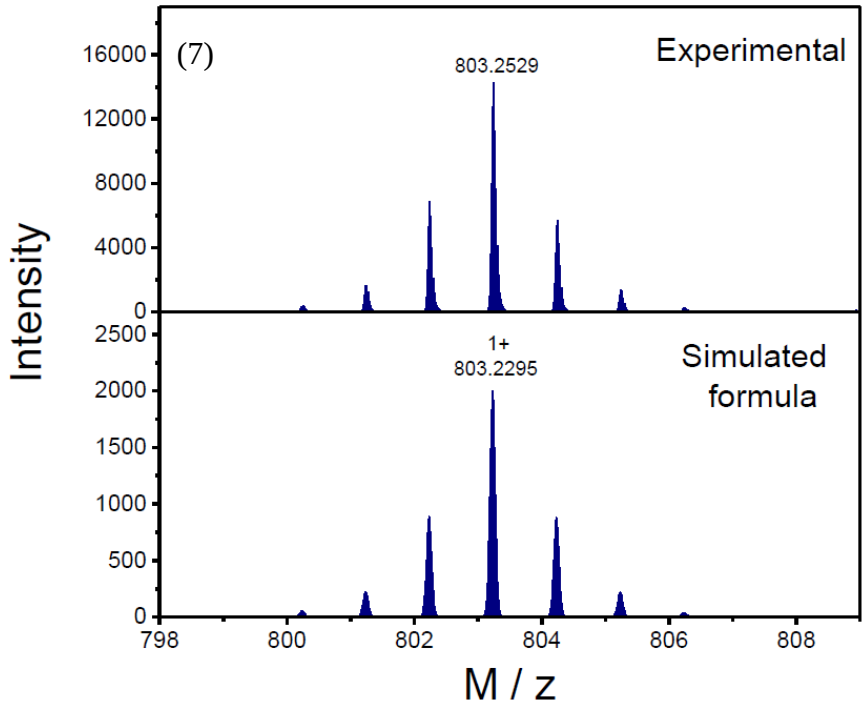
(7)
Experimental
803.2529
Simulated formula
1+
803.2295
Intensity
M / z

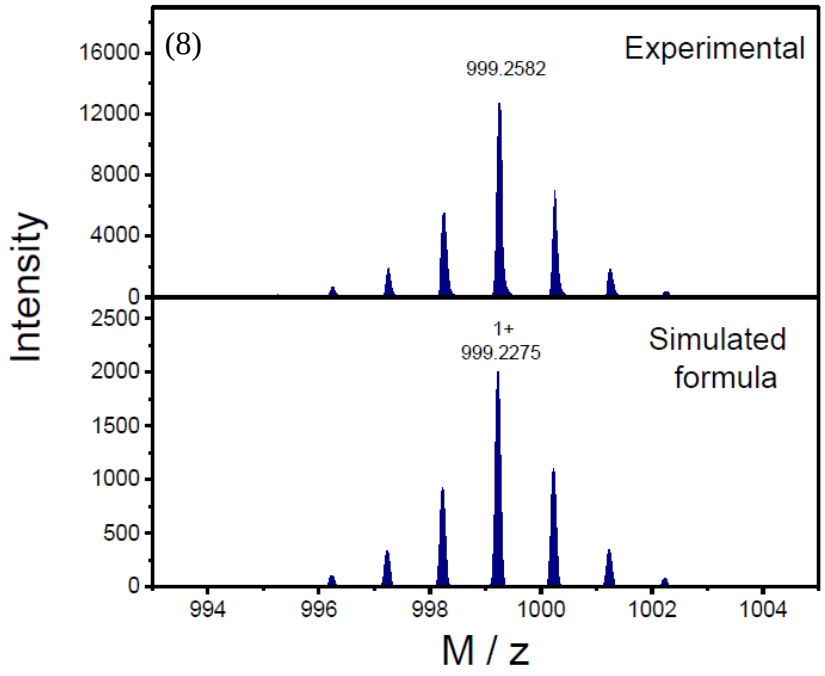


Figure B.2: HRMS for compounds 3-3 and BOPHY B (1, 4, 5, 6,)

Electrochemistry:

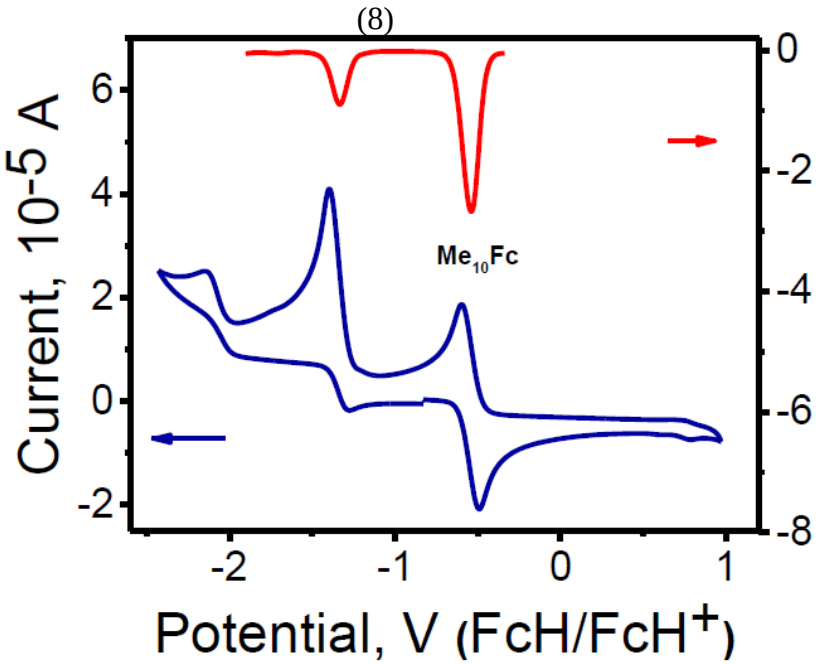

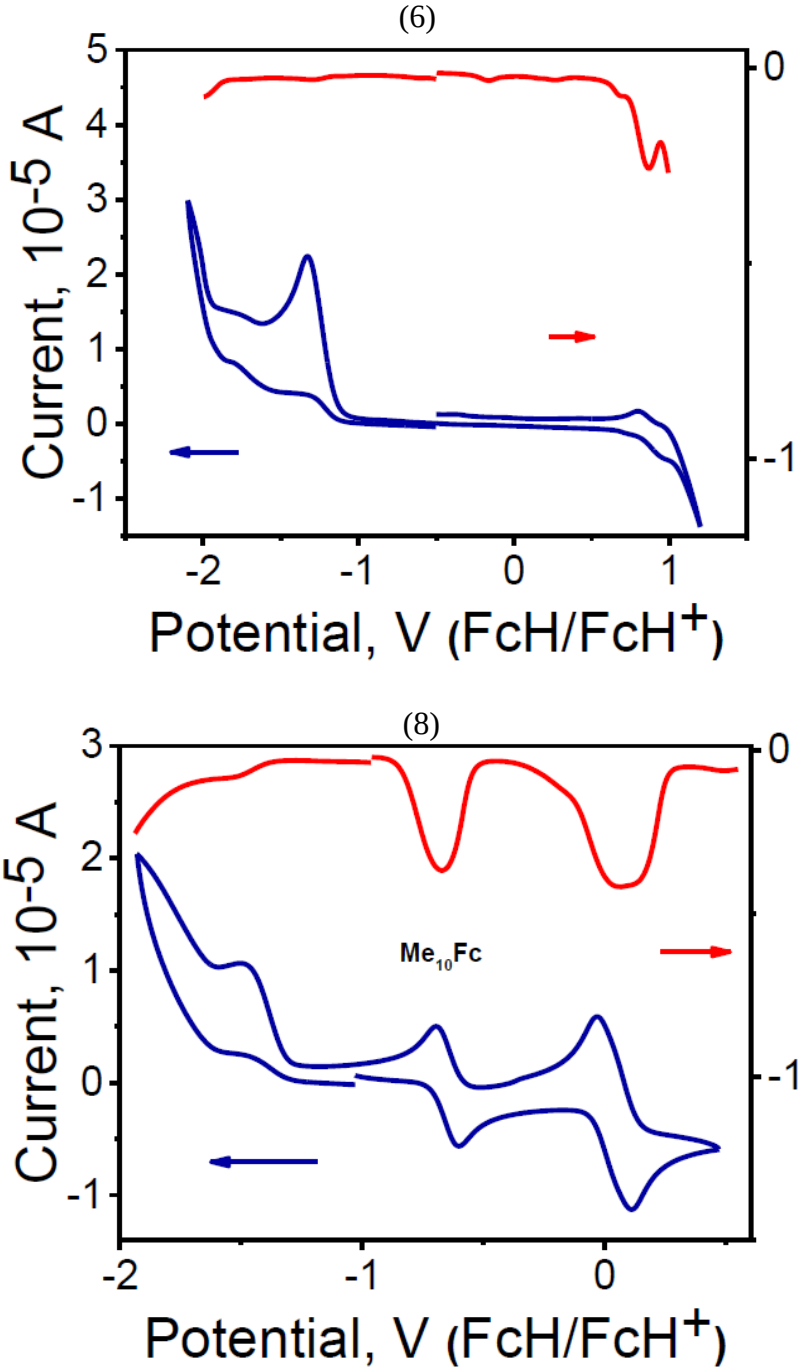


Figure B.3: DPV (top) and CV (bottom) voltammograms of BOPHY B- (1, 4, 6) in 0.1 M DCM/TBAP system

Spectroelectrochemical graphs:

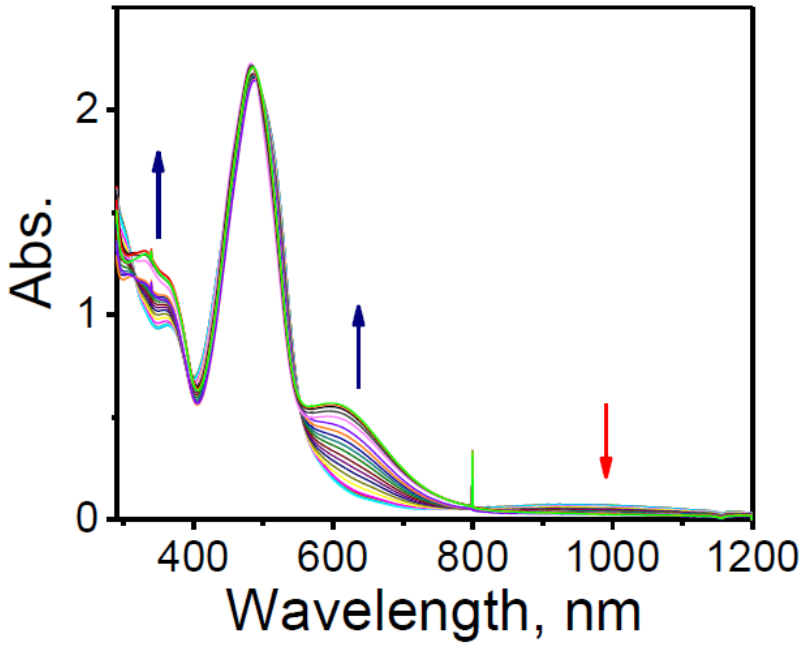


Figure B.4.1:Spectroelectrochemical reduction of 7 in 0.15 M

DCM/TFAB solvent system.

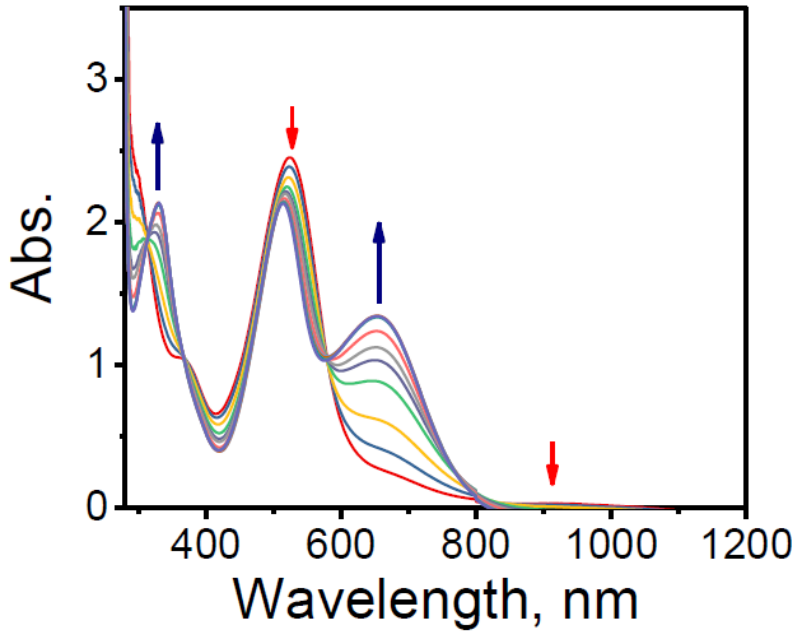

Figure B.4.2: Spectroelectrochemical reduction of 8 in 0.15 M DCM/TFAB solvent system. Table B.6.1: Optical and redox properties of BOPHY B compounds in DCM; Referenced with $FcH/FcH^+$

(a) = DCM/0.1M TBAP system, (b) = DCM/0.05M TBAF system

| Compound | λabs., nm (ε·10–3,M–1·cm–1) | Oxidation | | Reduction |
|---|---|---|---|---|
| | | $E_{1/2}^{Ox2}$,V | $E_{1/2}^{Ox1}$,V | $E_{1/2}^{Red1}$,V |
| 3 | 454(50.5), 473 (51.1) | - | - | -1.34 |
| 6 | 478(49) | - | ~0.80 | -1.3 |
| 7(a) | 498(28.5, 606(9.4) | - | 0.10 | -1.34 |
| 8(a) | 514(42), 656(32) | 0.10 | 0.10 | -1.28 |
| 8(b) | - | 0.150 | 0.08 | -1.4 |

Molecular Orbital

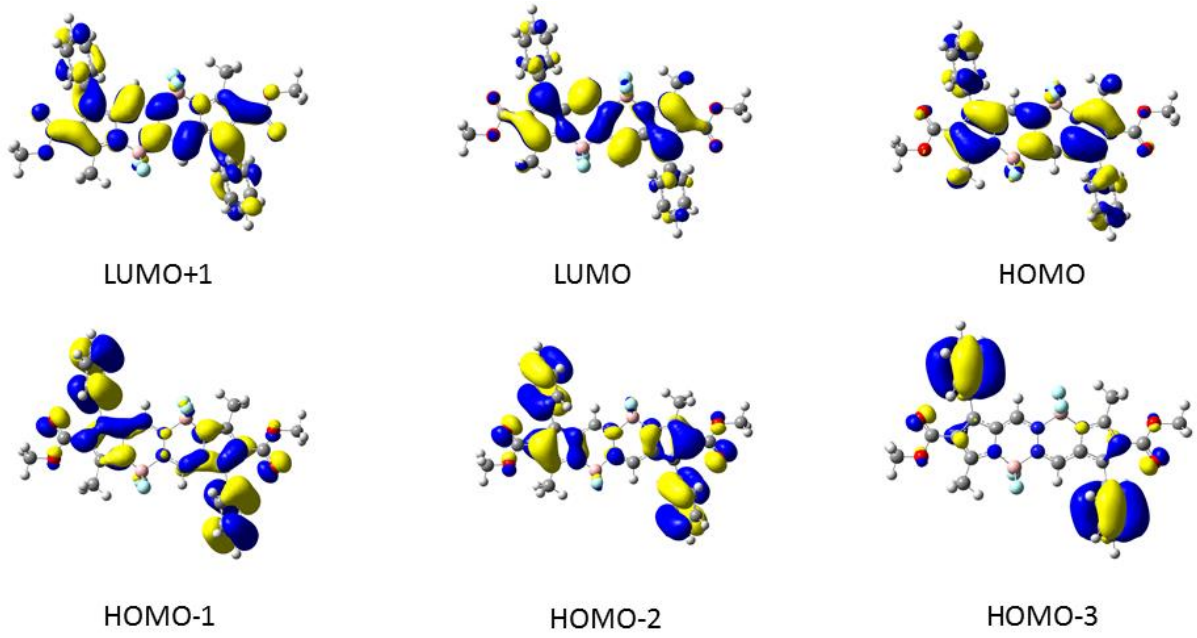


Figure B.5.1: DFT-calculated molecular orbitals for **3**.

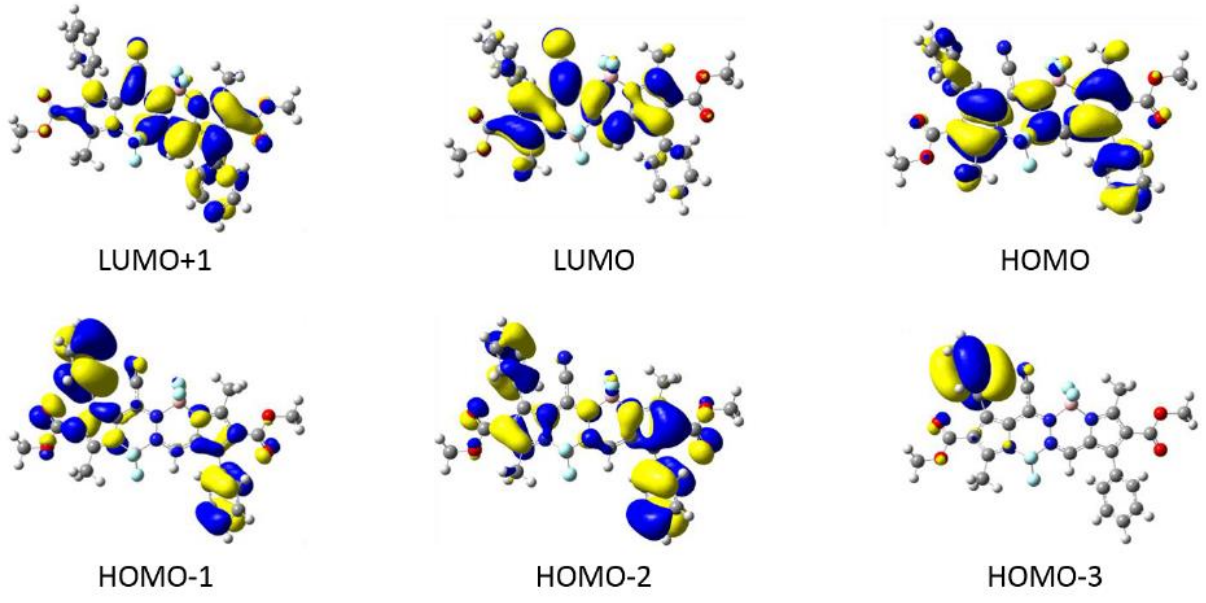


Figure B.5.2: DFT-calculated molecular orbitals for **5**.

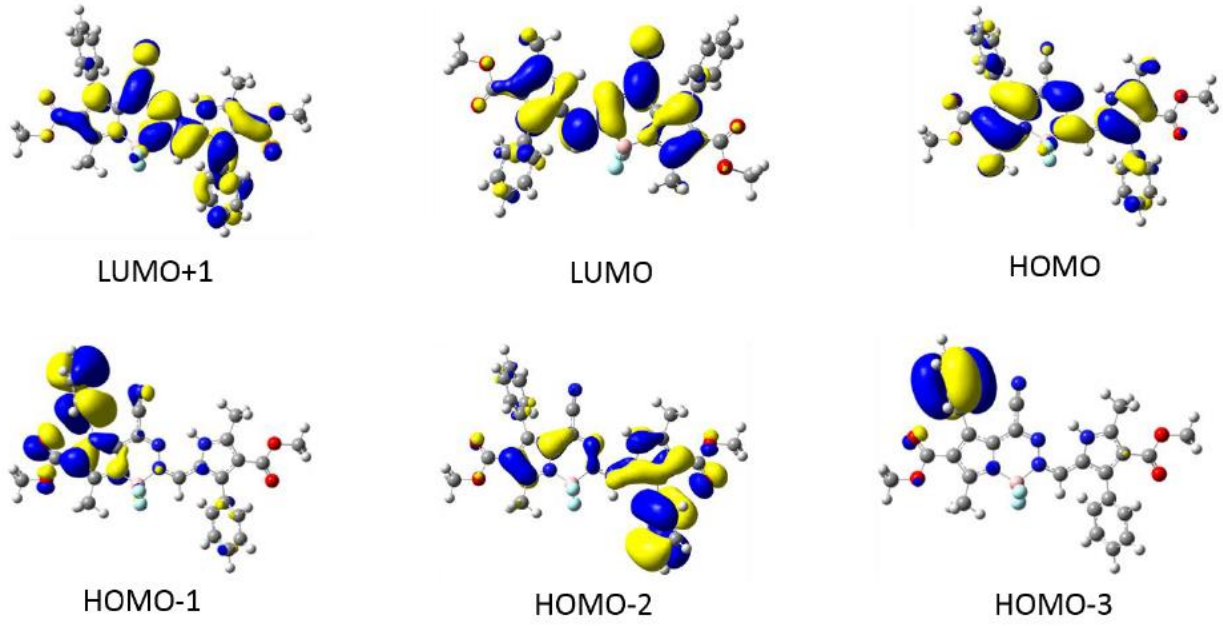


Figure B.5.3: DFT-calculated molecular orbitals for **6**.

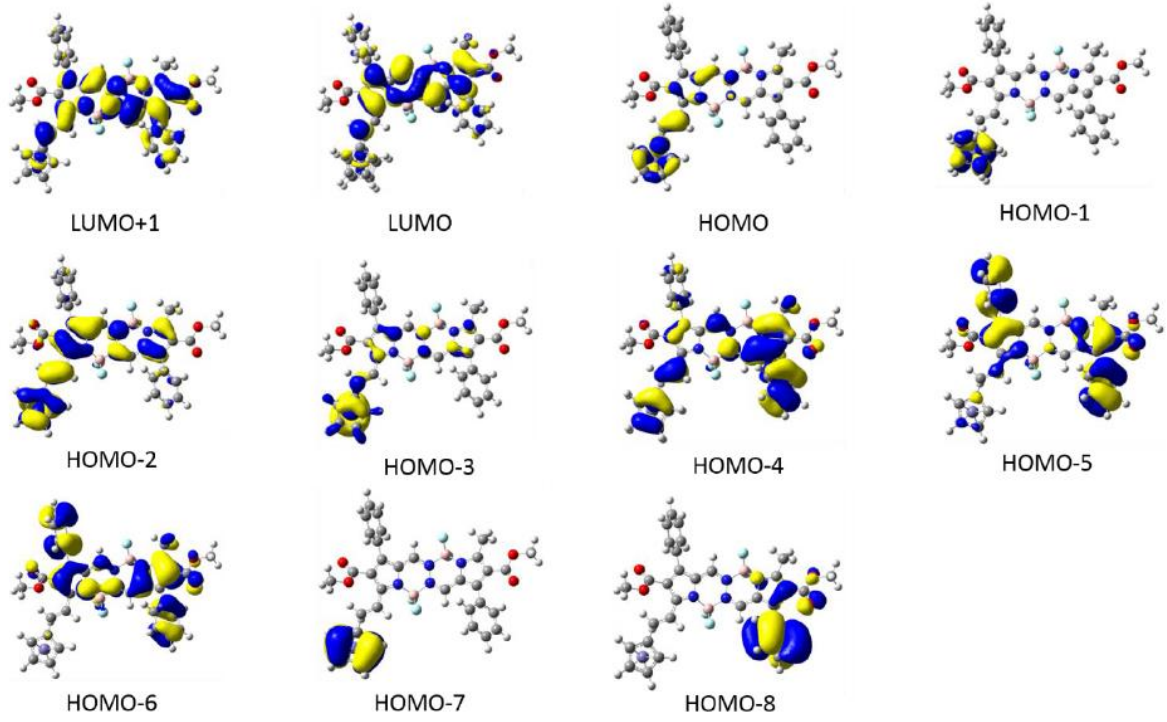


Figure B.5.4: DFT-calculated molecular orbitals for **7**.

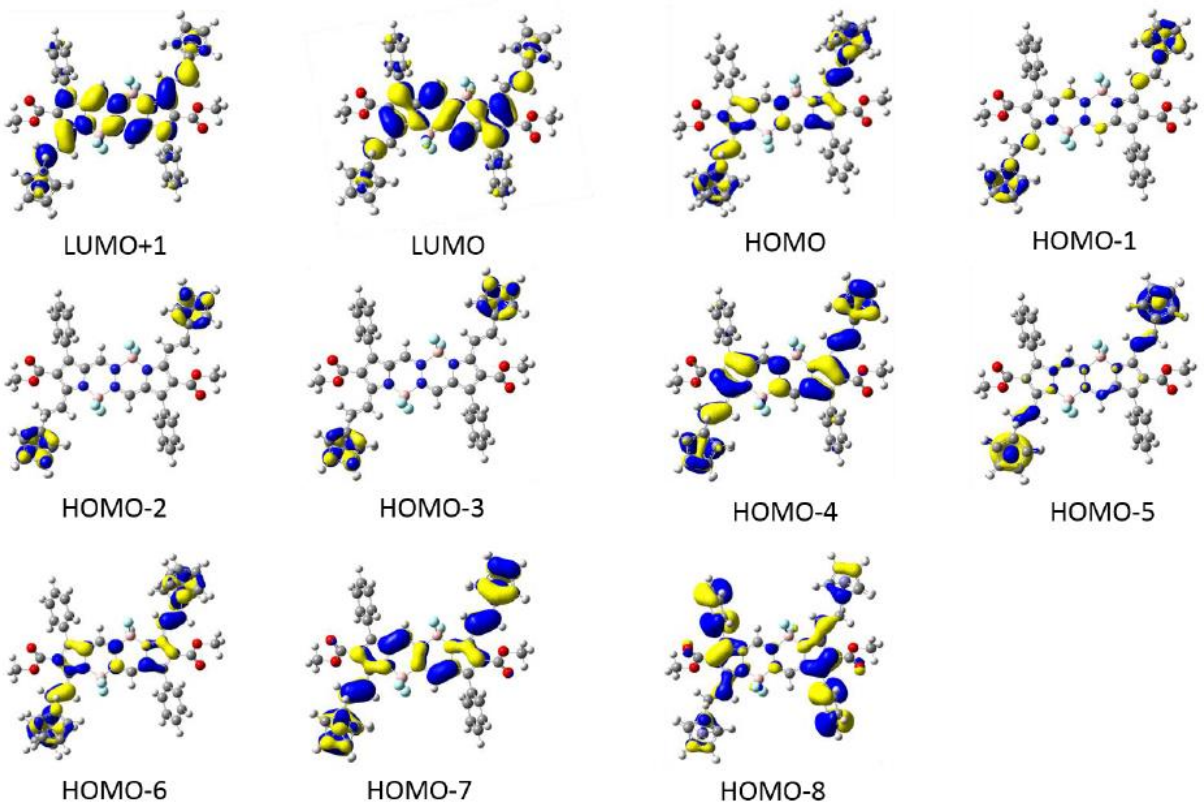


Figure B.5.5: DFT-calculated molecular orbitals for **8**.

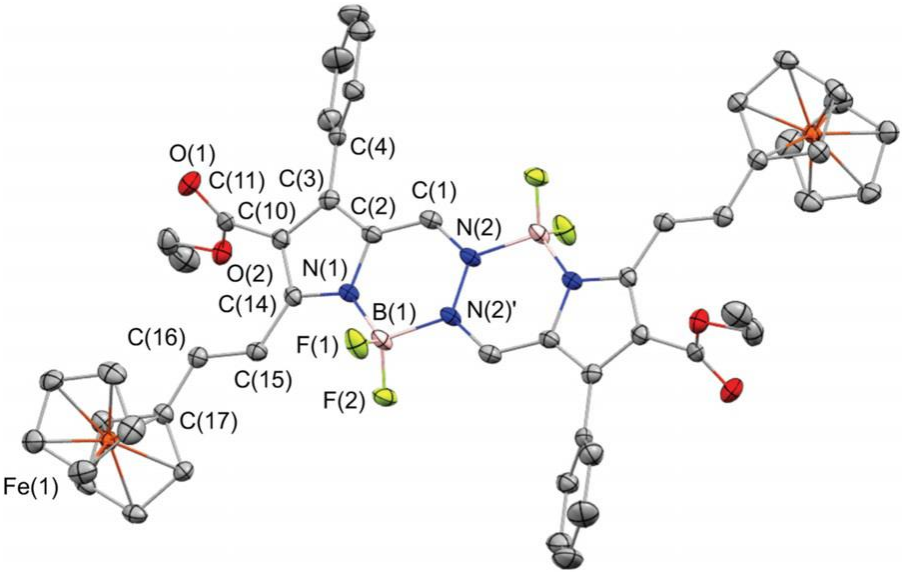


Figure B.6.1: ORTEP of Compound **8** with ellipsoids shown at 50% probability level.

Additional X-ray crystallography data can be found in the main text.[20]

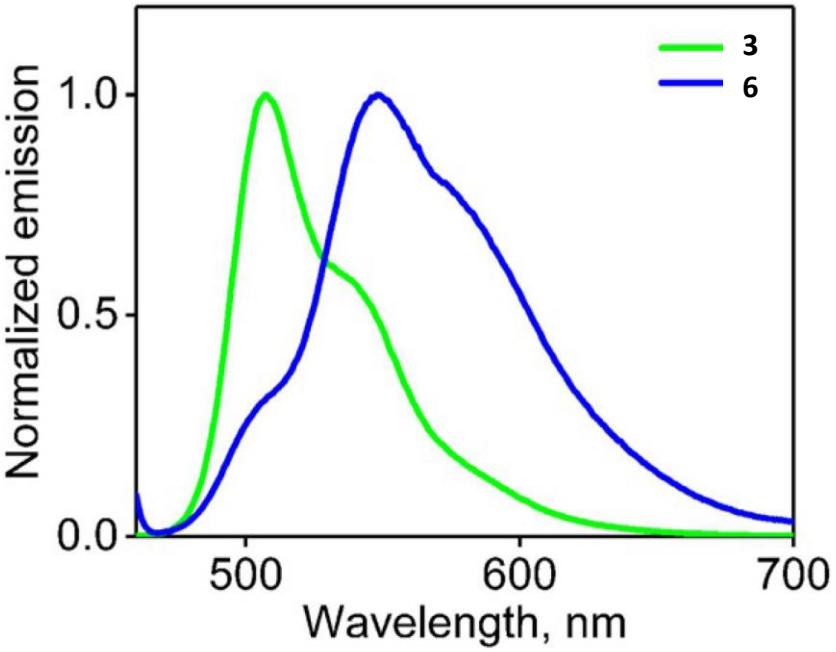


Figure B.6.2: Emission spectra for compounds **3** (green) and **6** (blue).

TDDFT Data can be found in the supporting Information for *Testing the Limits of the BOPHY Platform: Preparation, Characterization, and Theoretical Modeling of BOPHYs and Organometallic BOPHYs with Electron-Withdrawing Groups at b-Pyrrolic and Bridging Positions.*[20]